EINDHOVEN UNIVERSITY OF TECHNOLOGY

Eindhoven University of Technology

MASTER

Possibilities in failure analysis using a micro-Raman spectroscopy measurement system

van Spengen, W.M.

Award date:
1999

Link to publication

Disclaimer
This document contains a student thesis (bachelor's or master's), as authored by a student at Eindhoven University of Technology. Student theses are made available in the TU/e repository upon obtaining the required degree. The grade received is not published on the document as presented in the repository. The required complexity or quality of research of student theses may vary by program, and the required minimum study period may vary in duration.

General rights
Copyright and moral rights for the publications made accessible in the public portal are retained by the authors and/or other copyright owners and it is a condition of accessing publications that users recognise and abide by the legal requirements associated with these rights.

- Users may download and print one copy of any publication from the public portal for the purpose of private study or research.
- You may not further distribute the material or use it for any profit-making activity or commercial gain

POSSIBILITIES IN FAILURE ANALYSIS USING A MICRO-RAMAN SPECTROSCOPY MEASUREMENT SYSTEM

W. M. van Spengen

Graduate thesis
March 1999

IMEC vzw
MCP/MS/MSR
Kapeldreef 75
B-3001 Leuven
BELGIUM

Technische Universiteit Eindhoven
Faculteit Electrotechniek
Den Dolech 2
Postbus 513
5600 MB Eindhoven
THE NETHERLANDS

Supervisor: Dr. I. De Wolf (IMEC)
Erasmus coordinator: Dr. L. K. J. Vandamme (TUE)
Promoter: Prof. Dr. W. M. G. van Bokhoven (TUE)

POSSIBILITIES IN FAILURE ANALYSIS USING A MICRO-RAMAN SPECTROSCOPY MEASUREMENT SYSTEM

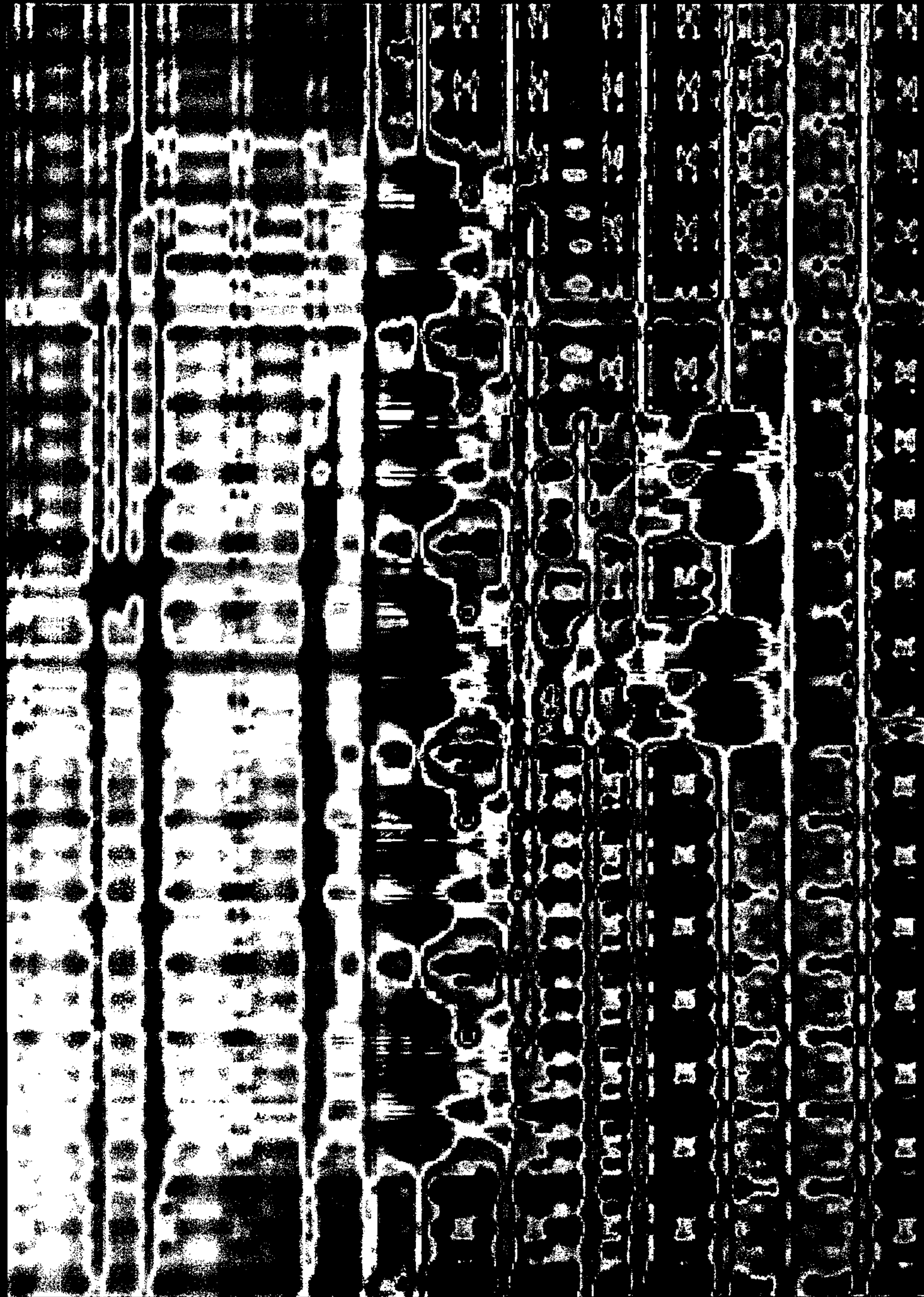

W. M. van Spengen
Graduate Thesis
March 1999
IMEC - Leuven, Belgium
Eindhoven University of Technology, The Netherlands

Summary

In this thesis, we will have a look at some improvements for the micro-Raman spectroscopy measurements and changes in the system setup to perform different kinds of measurements in the micro-electronic failure analysis domain. A brief overview of the different modern failure analysis techniques is given. The advantages and disadvantages of optical failure analysis techniques are discussed.

With a micro-Raman spectroscope it is possible to do mechanical stress measurements with a spatial resolution of less than a micron. To perform measurements on samples with large height differences a very accurate auto-focus system is needed. In this work, an *auto-focus system* has been developed in such a way that its control electronics can also be used to do a variety of failure analysis measurements. The auto-focus system makes use of the laser light reflected from a sample under the microscope of the micro-Raman spectrometer. This light is focused through a pinhole on a photodetector. The light intensity on this detector is high when the sample is in focus on the microscope and lower if it is out of focus: the intensity distribution as a function of objective position resembles a Lorenz function. The intensity peak is used for the focusing of the objective by the auto-focus module, which uses a piezo nanopositioner to move the objective to the right focus position.

By curve-fitting the intensity distribution along the focusing axis, we can estimate the top of the intensity distribution with high precision: this is our focal plane, and hence we can calculate the objective to sample distance. If we collect these intensity distributions on different positions on the sample, we might acquire a very precise *height map* of the sample.

The spatial resolution in the focal plane is determined by diffraction of the laser light, and is shown to be substantially improved by *digital image enhancement* techniques. Ordinary deconvolution techniques are used to prove that the resolution can indeed be improved this way, and blind deconvolution is suggested as a possibly useful alternative to this technique.

Instead of monitoring a photodetector, the auto-focus acquisition electronics can also be used to monitor the voltage across a constant current supply. If this current source is connected to the power terminals of an IC, and a focused laser beam is scanned over the surface of the sample, Light Induced Voltage Alteration (*LIVA*) images are obtained. Temperature Induced Voltage Alteration (*TIVA*) images could be obtained if a long wavelength laser and a differential preamplifier are used.

Finally, Kerr Rotation based Current Measurement (*KRCM*) is proposed to measure currents flowing in metal lines .

Table of contents

Summary 1
Table of contents 2
Introduction 5

PART ONE - Introduction to micro-Raman spectroscopy and failure analysis 6

Chapter one – Micro-Raman spectroscopy theory 7
Par 1.1 Rayleigh and Raman scattering 7
Par 1.2 The effect of stress upon the Raman spectrum of silicon 8
Par 1.3 Measuring stress with micro-Raman spectroscopy 9

Chapter two – Failure analysis techniques 12
Par 2.1 Introduction 12
Par 2.2 Overview of existing failure analysis techniques 12
Par 2.3 The software simulation, design for failure analysis and design for testability approaches in VLSI 13

Chapter three – Optical non-destructive failure analysis techniques 15
Par 3.1 The current status in optical non-destructive failure analysis 15
Par 3.1.1 Optical microscopy 15
Par 3.1.2 Infrared microscopy 15
Par 3.1.3 Scanning optical microscopy 15
Par 3.1.4 Light induced voltage alteration (LIVA) 16
Par 3.1.5 Temperature induced voltage alteration (TIVA) 16
Par 3.1.6 Optical beam induced current (OBIC) 16
Par 3.1.7 Optical beam induced resistance change (OBIRCH) 16
Par 3.1.8 Emission microscopy 16
Par 3.1.9 Micro-Raman spectroscopy 16
Par 3.2 Advantages and disadvantages of optical techniques 17
Par 3.3 New possibilities in optical failure analysis 17

PART TWO – Theory and applications 18

Chapter four – Principle and theory of the optical height measurement system 19
Par 4.1 Introduction 19
Par 4.2 Basic principle 19
Par 4.3 Properties of a focused laser beam 20
Par 4.4 Detector calculations and the z-axis intensity distribution 23
Par 4.5 Statistics of the z-axis intensity distribution 26

Chapter five – Description of the height measurement system 30
Par 5.1 Introduction and system setup 30
Par 5.2 Requirements 31

Par 5.3 The piezo transducer 31
Par 5.4 Description of the electronics 32
Par 5.5 Brief introduction to the software 33
Par 5.6 Measurement results 34
Par 5.6.1 Performance of the A/D and D/A 34
Par 5.6.2 The PI control system 35
Par 5.6.3 Intensity profile 35
Par 5.6.4 Repeatability of the height measurement 37
Par 5.7 Conclusions and future work 37

Chapter six – The micro-Raman auto-focus system 38
Par 6.1 Description of he micro-Raman system 38
Par 6.2 Application of the auto-focus system 38
Par 6.3 Description of the auto-focus algorithm 38
Par 6.4 Results 39
Par 6.5 Conclusions and future improvements 42

Chapter seven – Expanding the measurement electronics to LIVA 43
Par 7.1 Carrier generation by light incident on a semiconductor 43
Par 7.2 The LIVA imaging principle 44
Par 7.3 Implementation in the micro-Raman setup 45
Par 7.4 Measurement software 45
Par 7.5 Measurement results 45

Chapter eight – Image restoration – The spatial approach 50
Par 8.1 Introduction 50
Par 8.2 Convolution and the PSF 50
Par 8.3 High emphasis filtering 51
Par 8.4 Program description 52
Par 8.5 Results 52
Par 8.6 Two-dimensional formulation 54
Par 8.7 Micro-Raman spectroscopy stress measurements with high emphasis 54

PART THREE - Proposals for future investigation 56

Chapter nine –Time discriminating TIVA with a short wavelength laser 57
Par 9.1 The principle of TIVA imaging 57
Par 9.2 Recombination of excess carriers 57
Par 9.3 Implementation of the TD-TIVA approach 58

Chapter ten – Blind deconvolution 59
Par 10.1Introduction 59
Par 10.2 Blind deconvolution for micro-Raman spectroscopy 59

Chapter eleven – Kerr rotation based current measurement 61

Par 11.1 Basic principle 61
Par 11.2 Resolution 61
Par 11.3 Proposals for practical implementation 61

PART FOUR – General conclusions 62

Appendix A. – The acquisition electronics circuit board 63
Appendix B. – Image reconstruction software 64
Appendix C. – Micro-controller software 65
Appendix D. – Micro-Raman spectroscopy auto-focus software 74
Appendix E. – Data acquisition software 76

Acknowledgements 83
References 84

Introduction

Local mechanical stress in micro-electronic structures can be investigated with high spatial resolution by micro-Raman spectroscopy. In this thesis, we will have a look at some improvements for the micro-Raman spectroscopy measurements and changes in the system setup to perform different kinds of measurements in the micro-electronic failure analysis domain. To get a feeling for the possibilities of micro-Raman spectroscopy, the first chapter is devoted to the theory and application of the "Raman effect". In the second chapter a short overview will be given on the different failure analysis techniques in use at present, and the position of optical non-destructive failure analysis herein.
To perform Raman spectroscopy measurements on a square micron, highly advanced equipment is used, including a computer controlled microscope and a high precision spectrometer. Because it is often required to perform measurements at different positions on a wafer, an auto-focus system is needed that is highly accurate to prevent out of focus images due to incorrect outlining of the sample, large height differences and other causes. Although auto-focus systems for micro-Raman spectroscopy are available, they are not accurate enough to be used in high precision measurements.
The additions to the micro-Raman measurements include the description and evaluation of a high precision auto-focus system, and digital image enhancement to improve the spatial resolution of the collected data. The other kinds of failure analysis measurements made possible by the changes suggested in this work are high resolution non-contact topography measurements, LIVA and TIVA (methods to find defects in failed ICs in a single scan over the entire area of the die), and a method to measure the current flowing through conductors on the chip. It is particularly interesting to see these measurements in combination with Raman spectroscopy, because the same equipment can be used.

PART ONE
Introduction to micro-Raman spectroscopy and failure analysis

CHAPTER ONE
Micro-Raman spectroscopy theory

§1.1 Rayleigh and Raman scattering

When a sample of a crystalline material is illuminated by a monochromatic light source, the light will be scattered. The main scattering mechanism is Rayleigh scattering. The photons of the incident light, with frequency ω_i will be absorbed by the electrons of the sample, forcing them to go into an excited state. The electron will fall back into the ground state by emitting a photon ω_s of the same wavelength as the incident beam, but in a random direction (see fig. 1). Thus, the scattered light has the same frequency as the incident light.

But the scattered light also contains components having a slightly lower frequency then the incident light. This is explained by the fact that the excited electron looses some of its energy to lattice vibrations (phonons) before falling down to the ground state and emitting a photon (Stokes Raman scattering). In the same way, the excited electron can gain a little amount of energy by interaction with these lattice vibrations, so the photon emitted has a wavelength a little shorter than the incident light (anti-Stokes Raman scattering). Thus two (or more) new frequencies are generated by the interaction of the electron with the lattice in which it is contained, both higher and lower than the incident frequency. In molecular materials, the molecule vibrations achieve the same result [6].

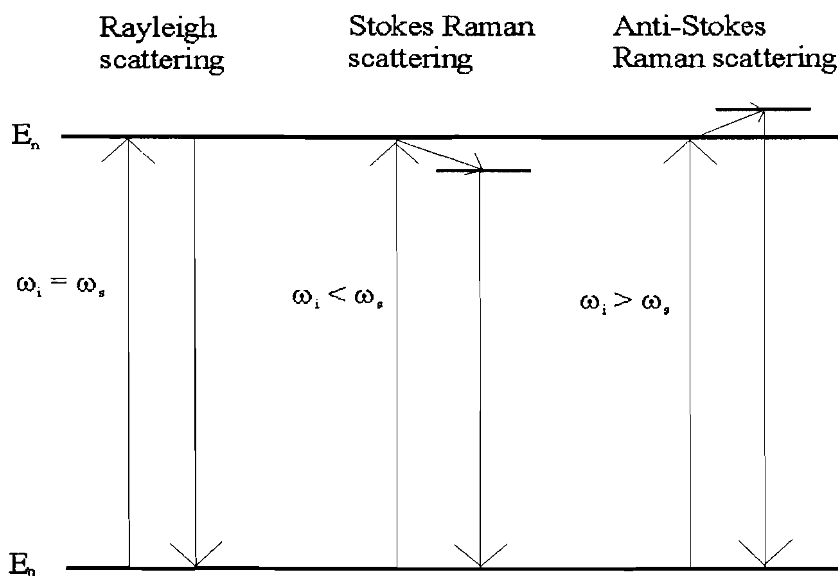

Fig 1.1 Raman scattering

The amount of shift is characteristic for the material, like its infrared spectrum, and the Raman spectrum can be used in the same way to determine the material(s) in the sample. By investigation of the spectrum the composition, crystallinity and (in the case of some semiconductors) doping of our sample can be determined. The Raman-shift is affected by temperature and the amount of mechanical stress applied to the sample, and so micro-Raman spectroscopy can also be used to measure temperature or mechanical stress. It is

the possibility to measure mechanical stress, which makes Raman spectroscopy very attractive to the micro-electronic industries, because it is the only way to directly measure mechanical stress in ICs.

§1.2 The effect of stress upon the Raman spectrum of silicon

We will have a look at a more classical way of explaining Raman spectra to extract information from the silicon Raman spectrum concerning the mechanical stress present in the material.

Light with an electric field **E** is incident on the sample and will cause a polarization **P** to occur following

$$\mathbf{P} = \chi_e \varepsilon_0 \mathbf{E},$$

in which χ_e is the electric susceptibility and ε_0 the dielectric constant of vacuum. **E** is a wave, so we can write for the polarization

$$\mathbf{P} = \chi_e \varepsilon_0 E_0 \exp[i(\mathbf{k}\cdot\mathbf{r}-\omega t)],$$

with **k** the wave vector describing the propagation direction, **r** the position and ω the frequency of the monochromatic light. The electric susceptibility is not always constant, because it can change due to lattice vibrations. The amplitude of the j'th of all possible lattice vibrations (or *phonons*) can be described by

$$Q_j(\mathbf{r}) = A_j \exp[\pm i(\mathbf{q}_j\cdot\mathbf{r} - \omega_j t)],$$

in which $\mathbf{q}_j$ is the wave vector of the j'th phonon and A_j is its amplitude. If we neglect the effects when more than one phonon are involved (they are very weak), we can write χ_e in a first order Taylor expansion as

$$\chi_e = \chi_0 + \left(\frac{\partial \chi_e}{\partial Q_j}\right)_0 Q_j.$$

When we write the polarization **P** as function of the incident light (electric field **E**) and the non-constant susceptibility χ_e, we obtain

$$P = \varepsilon_0 \chi_0 E_0 \exp[i(k\cdot r - \omega t)] + \varepsilon_0 E_0 \left(\frac{\partial \chi_e}{\partial Q_j}\right) A_j \times \exp[-i(\omega \pm \omega_j)t] \exp[i(k \pm q_j)\cdot r].$$

We see that the re-radiated light will contain three components. The first is the light not shifted in frequency we already knew to be the Rayleigh scattered light. We also see a part radiated at a frequency lower than the incident light by an amount ω_j, and a part shifted upward by an amount ω_j. These are called the Stokes and anti-Stokes Raman frequencies, respectively. Note that for any Raman signal to be observed it is needed that

$\left(\frac{\partial \chi_e}{\partial Q_j}\right) \neq 0$, which means that the electric susceptibility changes if lattice vibrations or other kinds of disturbances are present. For crystalline materials, the intensity of the Raman scattered light depends on the polarization and the plane of incidence of the laser light. So by changing our plane of incidence, we will see different contributions to the Raman signal. If we have the laser beam illuminating the sample from the top side of a wafer, perpendicular to the surface, the scattering is from the (001) surface, and in that case only the z-polarized phonon will be observed.

Mechanical stress may change the frequencies of the Raman modes. In first order approximation, the frequency changes can be calculated from

$$\begin{bmatrix} p\varepsilon_{11} + q(\varepsilon_{22} + \varepsilon_{33}) - \lambda & 2r\varepsilon_{12} & 2r\varepsilon_{13} \\ 2r\varepsilon_{12} & p\varepsilon_{22} + q(\varepsilon_{33} + \varepsilon_{11}) - \lambda & 2r\varepsilon_{23} \\ 2r\varepsilon_{13} & 2r\varepsilon_{23} & p\varepsilon_{33} + q(\varepsilon_{11} + \varepsilon_{22}) - \lambda \end{bmatrix} = 0.$$

The p,q and r are material constants, the phonon deformation potentials, and the ε_{ij}'s are the strain tensor components. The eigenvalues λ give us the change in frequency:

$$\lambda_j = \omega_j^2 - \omega^2,$$

with ω the Raman frequency without stress and ω_j the shifted Raman frequency of the stressed material. By making some simplifications, calculating the strain tensor components using Hooke's law and observing the polarization selection rules we omit here, it is found for example for uniaxial stress in Silicon in the (001)-plane that

$$\Delta\omega\ [\mathrm{cm}^{-1}] \approx 2 \cdot 10^{-9} \sigma\ [\mathrm{Pa}].$$

So we can calculate the amount of uniaxial stress in a silicon sample from the shift in frequency of the Raman signal. A shift towards the laser line indicates tensile stress, while a shift away from it indicates compressive stress [24]. If stress is more than one direction is present, matters are somewhat more complicated, but it is possible to describe the Raman signal observed in this case theoretically as well [23].

§1.3 Measuring stress with micro-Raman spectroscopy

When a laser is focused on a silicon sample through an optical microscope with a high power objective, a focused spot of less then a square micron can be obtained. Because the Raman spectrum of only this small area is collected at once, the extracted stress data are collected only for this small part also. This means that by scanning across a die and collecting the Raman spectrum of all associated positions, a stress map of the die can be generated. The main problem is to get rid of the very intense Rayleigh scattered light, which is typically 10^{12} times as strong as the Raman scattered light. This is done using a double monochromator. The spectrum is unraveled in the spectrometer and the weak Raman spectrum is collected by a very sensitive liquid nitrogen cooled CCD detector.

The complete setup is given in fig. 2. A typical Raman spectrum of silicon, measured with this kind of equipment will look like the spectrum in fig. 3. Apart from the Raman peak of silicon, at 520 cm^{-1}, we see small plasma lines, generated by gas discharges in the laser tube. The characteristic peak in the Raman spectrum of silicon shifts towards higher frequencies when compressive stress is applied to the sample, and the Raman frequency will decrease with tensile stress.
The higher the frequency of the laser, the less the light will penetrate in the silicon, so with short wavelength lasers it is possible to measure the stress near the surface of the sample. This is the most important region, for stress is often the highest near the surface. Care must be taken that the laser power is not too high, for heating the sample will cause a downward shift of the Raman peak which has nothing to do with stress.
Because the stress-induced effect is quite weak, the whole peak in the Raman spectrum is fitted with a Lorenz function. The peak in this function will give the place of the peak in the spectrum. This method is better for exact determination of the shift than just looking for the peak in the spectrum without a mathematical aid. An example of the results of a stress measurement, in this case the stress in 2 μm broad and 100 nm thick silicon nitride lines on silicon, is given in fig. 4.

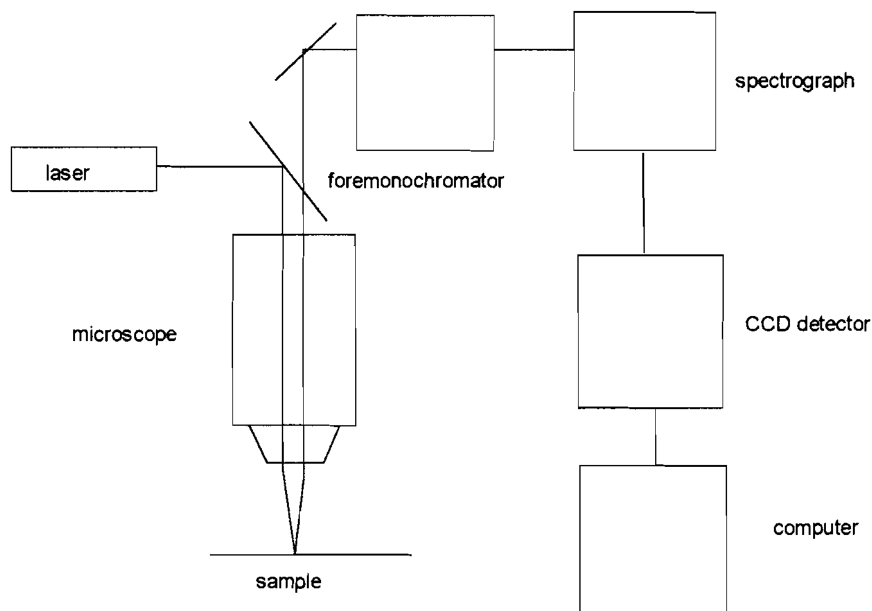

Fig 2. Micro-Raman spectrometry setup.

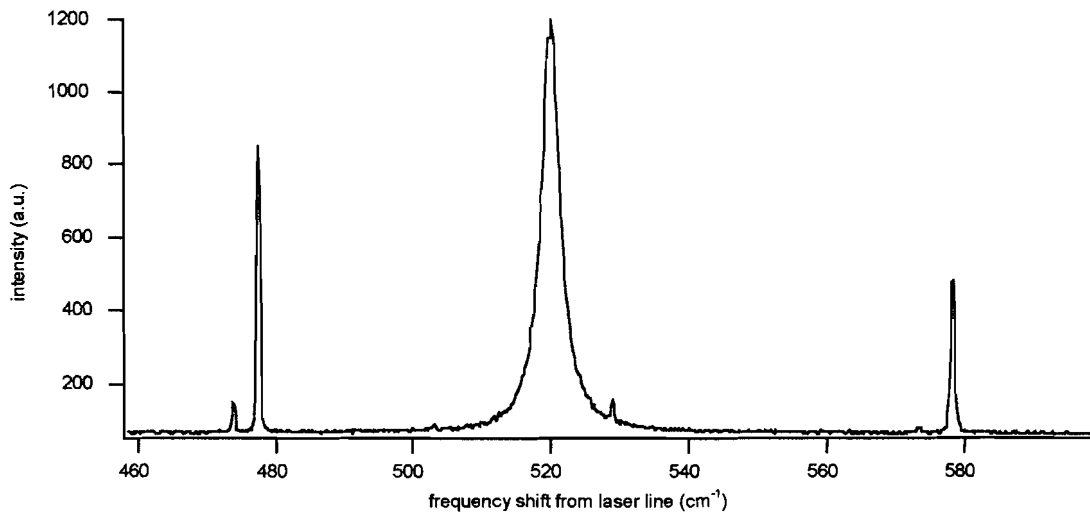

Fig 3. Raman spectrum of silicon with plasma lines.

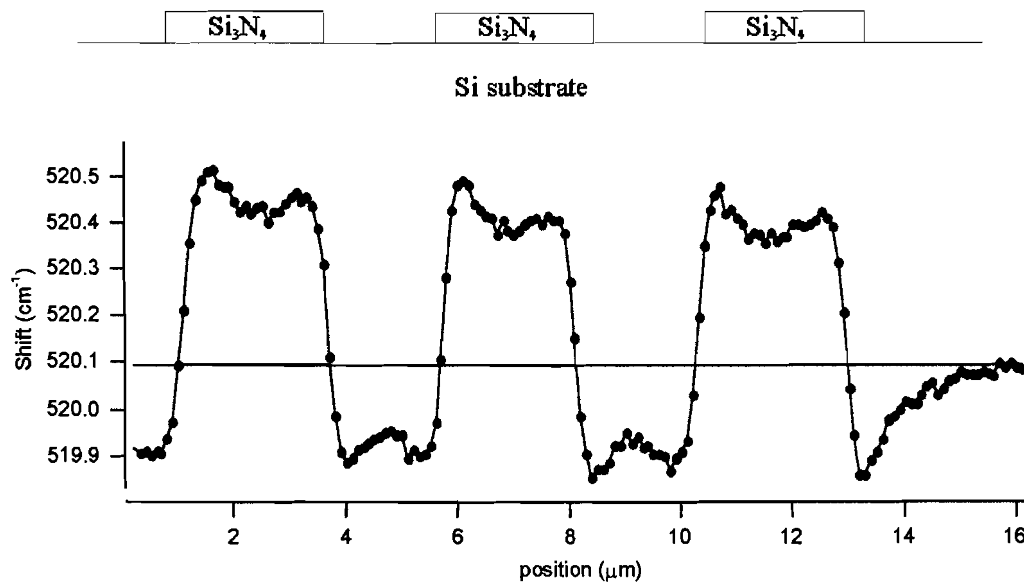

Fig. 4 Shift of the Raman peak due to stress while scanning over 2 μm silicon nitride lines.

CHAPTER TWO
Failure analysis techniques

§2.1 Introduction

Failure analysis is a very important part in the development of an integrated circuit. By providing the design and process engineers with the cause of a certain observed failure, corrective action can be taken to improve the design or process. We have to distinguish between fault detection, fault isolation and fault determination. Fault detection is the part involving the discovery and the exact description of the behavior of the integrated circuit with the error. After it is assured that there actually is an error, and after the error is documented, the fault isolation process is used to find the exact position on the die where the failure is expected to be coming from. When this position is found, fault determination is needed, to find the reason why the device is not functioning properly at that position. To achieve this, destructive techniques are often needed, to strip away unwanted layers which prevent the fault from being seen. On the other hand, finding the failure site (fault isolation) can be often accomplished without relying on techniques which damage the sample. Sophisticated equipment is needed to perform this task, and a large part of this report is devoted to the improvement of existing methods and the description of new techniques which might turn out to be very useful in the fault isolation process. Because a micro-Raman measurement system was already available at the beginning, the components of this piece of equipment had to be the basis of the to be developed "new" measurement setups. Also, a high accuracy microscope auto-focus for this system was needed. The usable parts for a new measurement setup include a high power, short wavelength laser, a computer controlled XY-stage, an optical microscope, and a micro-Raman spectrometer. Because a (high power) laser and a computer controlled microscope are used for most optical failure analysis techniques, and also because of their cost, this turned out to be a very reasonable starting point.

§2.2 Overview of existing failure analysis techniques

We will first have a look at the different techniques which are in use by the failure analysis engineers nowadays. It is not pretended that this list is exhaustive, nor will we have a look on all the possibilities. The interested reader will find more information, and a very useful reference list in [20]. Here we want to get some feeling for the field in which the optical failure analysis techniques are used, and what role they play in comparison with the other techniques available for this purpose.
All these techniques have their own field of application. The electronic measurements are mostly used to define the actual behavior of the failing device. A lot of problems are still discovered to be due to electrostatic discharge (ESD) and electrical overstress (EOS).

The main techniques are listed in table 1.

TABLE 1

technique or tool	**Examples**
electrical measurement techniques	curve tracing, I_{DDQ} test (quiescent current)
optical techniques	optical/ infrared/ scanning microscopy, light/ temperature induced voltage alteration, optical beam induced current/ resistance change, micro-Raman spectroscopy
physical techniques	mechanical probing and cutting, layer removal, deprocessing, cross sectioning
thermal imaging techniques	liquid crystals, infrared/ fluorescent microthermography [1]
electron beam techniques	secondary electron, backscattered electron, X-ray, (capacitive coupling or with I_{DDQ}) voltage contrast, electron beam induced current, (biased) resistive contrast imaging, (low energy) charge induced voltage alteration, Auger electron spectroscopy
light emission microscopy	IR and visible light
ion beam techniques	focused ion beam, secondary ion mass spectroscopy
scanning probe microscopy	atomic force, scanning tunneling, magnetic force

The fault determination process benefits from high resolution and may well involve destructive techniques to free buried layers in which the defect might be present. Physical techniques and ion/ electron beam techniques are used to remove and investigate the layers at the failure site. Except for mechanical stress measurements with micro-Raman spectroscopy, for which no real non-optical alternative is available, this is not the field in which optical techniques have much to offer. High resolution can be achieved with an electron microscope, and with its special versions for failure analysis a lot of useful measurements can be performed. Even the voltage of the conductors on the die can be measured using an electron beam. Care has to be taken that the sample is not damaged by the highly accelerated electrons. The unwanted newly implanted charge in the gate oxide can also change the threshold voltage of a transistor considerably. If desired, still higher resolution can be achieved by some of the scanning probe techniques.
These high resolution techniques however, generate too much information to be useful in the fault localization process. In this part of the failure analysis chain, inspection of the entire die in a single scan would be preferable. To prevent one from becoming overwhelmed with data, a technique must be used which only generates a signal at the fault position. It is this part of failure analysis in which the optical techniques have much to offer. The microthermal techniques are also useful here, but they can only be applied if the defect causes the generation of heat.

§2.3 The software simulation, design for failure analysis and design for testability approaches in VLSI

With the ever increasing density and miniaturization of the structures on an integrated circuit, it turns out that a lot of techniques commonly used for failure analysis cannot be

applied anymore. This is because of the multiple metal layers which effectively screen the active regions, and also because structures have become so small as to render the usual optical microscope measurements unusable due to lack of resolution. To partly circumvent these limitations, software simulation can help in the fault isolation process, and the circuit can be designed in such a way that the most important conductors are always accessible [13].
Special circuit parts are added in the design to enlarge the test possibilities. In new microprocessors, special externally accessible microcode registers are added to debug processors with a microcode failure. Memory arrays can be read out with an Array Dump Tool, and the contents can be compared with a simulation of the same microprocessor state. The most important control signals can be read out with a Test Access Port instruction and a "Scanout" tool. Special test modes are added for easy software access to the arrays under test. The development and buying of expensive test equipment can be reduced by a programmable built-in self test, which integrates the required test systems into the chip itself.
Simulation with a model of the microprocessor can also add very useful information in the failure isolation process.
With the expectations for the transistor count in future generations of microprocessors it is assumed that these "non-physical" techniques will become even more important. However, on the process development level, the need for accurate "physical" techniques will remain and even increase.

CHAPTER THREE
Optical non-destructive failure analysis techniques

§3.1 The current status in optical non-destructive failure analysis

We will now have a look at the currently used optical non-destructive failure analysis tools. In table 2 these techniques are presented .

TABLE 2

Technique	**paragraph**
optical microscopy	1.1
infrared microscopy (front side and back side)	1.2
scanning optical microscopy (SOM)	1.3
light induced voltage alteration (LIVA)	1.4
temperature induced voltage alteration (TIVA)	1.5
optical beam induced current (OBIC)	1.6
optical beam induced resistance change (OBIRCH)	1.7
emission microscopy	1.8
micro-Raman spectroscopy	1.9

§3.1.1 Optical microscopy

The easiest to use and probably oldest piece of failure analysis equipment is the optical microscope. It is still widely used for investigation of the sample surface. Because of the wavelength used (in the visible region) its resolution is diffraction limited to about half a micron (see chapter four). The easy way in which it can be used makes it a very attractive tool for observing physical properties of structures which are not too small.

§3.1.2 Infrared microscopy

In infrared microscopy the visible illumination source is exchanged with an infrared one. This offers the possibility to look from the back side of the die, because silicon is transparent to wavelengths larger than about one micron. The advantage is that the metal layers do not obscure the active regions, and that "flip-chip" (upside down) packaged IC's can also be investigated. Its main disadvantage is its poor spatial resolution. Because of the long wavelengths involved, the spot is usually more than one micron in diameter. This is the limiting factor in the use of IR microscopy for new generations of microprocessors.

§3.1.3 Scanning optical microscopy

The confocal scanning optical microscope offers a somewhat better resolution and a larger depth of focus than an ordinary microscope. This is because of the fact that in the confocal imaging mode, the resolution is determined by the square of the point spread function (spot size intensity distribution, see chapter 4).

§3.1.4 Light induced voltage alteration (LIVA)
LIVA images are produced by scanning a focused short (visible) wavelength laser beam over the sample and monitoring the IC supply voltage when powered by a constant current source. The photons have a higher energy than the silicon bandgap, and generate electron-hole pairs. When the recombination current of these carriers affects the operating current of the IC, a LIVA signal is observed. This is the case if the carriers are generated near a Fermi-level change. This technique can be used to find open circuits and for transistor logic state mapping. In chapter seven, we will have a close look at LIVA and in chapter nine at its long wavelength counterpart, TIVA

§3.1.5 Temperature induced voltage alteration (TIVA)
When the wavelength of the laser in a LIVA system is so long that carriers cannot be generated, the only effect of the focused laser beam is locally heating the die. This induces carriers in the conductors due to the thermocouple effect. When the conductor is connected to a low resistance bus the generated voltage will disappear immediately, but when it is floating due to an open circuit, the state of the transistors connected to it will change. This changes the IC power demand, and a very weak TIVA signal is observed. The heating of a short circuit will change its resistance en hence also affect the device quiescent current. This technique can be very effectively used to perform measurements from the backside of an IC, e.g. for flip-chip packages.

§3.1.6 Optical beam induced current (OBIC)
OBIC is an older variant of LIVA, in which the current demand of the IC is measured using a constant voltage supply [3].

§3.1.7 Optical beam induced resistance change (OBIRCH)
When a metal line is locally heated with a focused laser beam, the heat will be transmitted more to the surroundings when the line is correct, but will stay and increase the resistance of the line, if the heat cannot flow away due to defects such as voids in the metal. This resistance change affects the current through de line when a constant voltage source is applied. This technique is was never used for actual devices due to the also generated much stronger OBIC signal. Now and then, selective area scanning (SAS-) OBIRCH is used to investigate parts of a sample which do not generate OBIC signals [15].

§3.1.8 Emission microscopy
Failure sites that generate light during chip operation can be found with emission microscopy (EMMI). The failure site emits faint light due to recombination or energy level changes of carriers which can be seen by an appropriate detection system. Because the whole die can be investigated at once this is a very useful tool to find failures sites.

§3.1.9 Micro-Raman spectroscopy
The position of the characteristic silicon peak in a Raman spectrum changes with the amount of mechanical stress in the structures. With a scanning optical microscope it is possible to focus the laser beam to a small spot and do stress measurements with a spatial

resolution of less than a micron. Micro-Raman spectroscopy can also be used to study local composition, crystallinity, doping and temperature. A more elaborate treatment on this topic was given in chapter one.

§3.2 Advantages and disadvantages of optical techniques

We have seen in the preceding paragraph that optical techniques have much to offer for failure analysis. The main advantages are their inherent non-destructiveness (except at extremely high laser powers) and their (in most cases) relatively modest cost.
The most important disadvantage of optical techniques is their relatively large probing spot, and hence their limited resolution. Shorter wavelengths (UV), and the use of high refractive index optics (oil immersion lens and solid immersion lens (SIL)) can improve this somewhat, but are not likely to ever give a detailed view in the 100 nm region or less. Near-field scanning optical microscopy (a scanning probe technology) is expected to improve matters a little in the future, but the problem with this technique is its low efficiency. For measurement techniques that rely on effects only to be observed when a lot of photons are used (micro-Raman spectroscopy, TIVA, OBIRCH), this will probably never be a real alternative for the commonly used laser beam which is focused through a high power microscope objective.
However, the real situation is less bad. Conductors smaller than the resolution of a LIVA or TIVA system will still be visible, but the structure which generates the signal will appear larger in the image than it actually is. But as we just want to locate the fault, this is not really a problem.
For a lot of the previously mentioned techniques, it is important to notice that the observed effects are very weak, and that sensitive detectors and long acquisition times are required to see anything at all.

§3.3 New possibilities in optical failure analysis

To further enlarge the possibilities of optical failure analysis, a couple of improvements and new measurement techniques are suggested. These will be covered in detail in the next parts of the report. The first is a high resolution height measurement system, which is basically a non-contact profilometer with a high z-axis resolution. It can also be used as a micro-Raman spectrometer auto-focus system. The second is *digital image enhancement*, which corrects for the lack of spatial resolution when using optical techniques by counteracting the effect of the point spread function (spot size) of the imaging system.
Third, we will show that it might be possible to do *TIVA with a short wavelength laser*, which improves the spatial resolution of this technique considerably and does not require an expensive far infrared laser. The last part briefly discusses a completely new technique, *Kerr Rotation based Current Measurement* (KRCM). This technique may allow us to measure the current flowing through each individual conductor on the die by spinning a thin film on the surface, which is then magnetized by the current flowing through the conductor.

PART TWO
Theory and applications

CHAPTER FOUR
Principle and theory of the optical height measurement system

§4.1 Introduction
A lot of faults in a micro-electronic circuit can be found by inspection with an optical microscope. Quite often one is not only interested in the lateral dimensions on the chip, but also in the height of the structures. It would be really an improvement of any optical failure analysis measurement system if a height measurement possibility was available with a reasonable resolution compared to the height of the micro-electronic structures. A couple of different profilometers exist, but they are very expensive, their resolution is often limited [5] and many of them require some kind of contact between the profilometer and the sample. As in our case, the light-based high resolution systems are mainly used to investigate slowly varying height differences and not sharp edges, because the resolution is better along the z-axis than in the xy-plane.
So, not only from the perspective of the availability of the components of the micro-Raman spectroscopy system, but also as a new stand alone device, there is room for a measurement system which can perform accurate height measurements with reasonable precision without becoming too expensive or requiring specially prepared samples. The disadvantage is that it can never be as precise for certain measurements as dedicated techniques like atomic force microscopy. But for all other applications such a piece of equipment would be very promising if it could be constructed.
Commercially available profilometers have been constructed with a typical resolution up to a couple of nanometers (e. g. Zeiss, UBM). These use the special properties of interference to achieve the very high accuracy required. This type of equipment is rather expensive. Here we will describe a new approach to height measurements with a possibly very high resolution which can be constructed at a relatively modest cost if needed, although in our case it is part of the already available micro-Raman spectroscope .

§4.2 Basic principle
With a laser and a computer controlled microscope it is possible to do height measurements by changing the objective height until it is in focus, and saving the data associated with this position. By scanning the entire surface in this way a height map of the device under test can be constructed. However, this method of measuring height is very crude, because the exact focal position cannot be measured accurately. This is due to the fact that diffraction tends to broaden the area in which the objective focus is almost constant compared to what one would expect from geometrical optics.
The light generated by a laser is focused on the sample through an optical microscope. The reflected light is split by a partially reflecting mirror (10% is reflected) and focused again on a photodetector (see fig. 1). The intensity is high when the sample is in focus under the microscope. We detect the position of the focal plane by moving the objective through the focal plane and watch the light intensity on the detector.

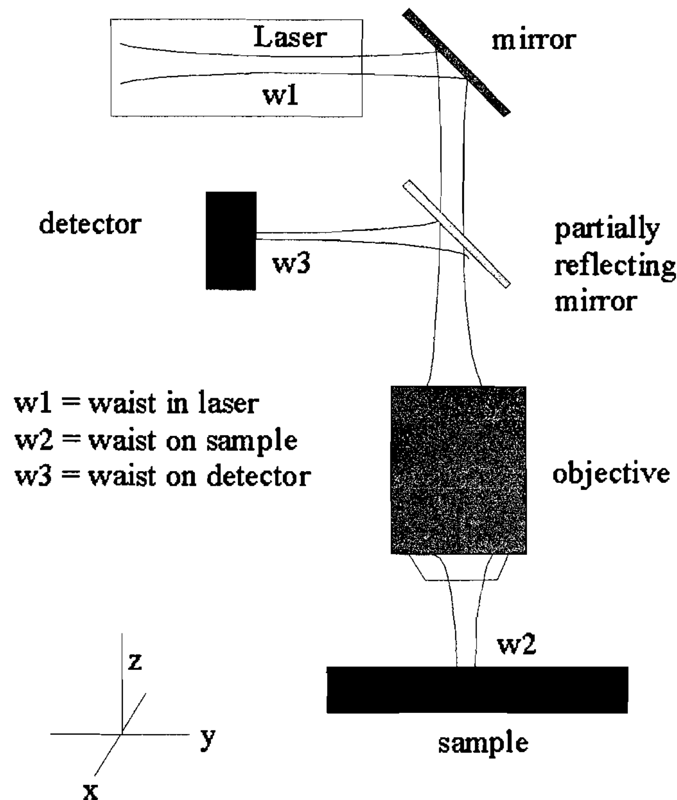

Fig. 1. Measurement setup

By collecting all the data of the position of the objective and the corresponding reflected laser light intensity, when it is moved through the focal position, and using all this data to calculate the position in which the best focus was found, this position can be found much more precise by curve fitting. In that case, all the data are fitted with a mathematically described curve, to determine the exact position of the highest intensity. Disadvantage is the fact that a lot of data is generated for very large area's, gigabytes being not unusual. This amount of data cannot reasonably be saved for later data manipulation, but must be processed runtime during the measurement. In this chapter we will have a look at the theoretical principles behind such a 3D optical microscope.

§4.3 Properties of a focused laser beam

When a laser beam propagating along the z-axis is focused by means of a high power microscope objective to a sample in the xy-plane, see fig. 1, we find that the focused light does not behave as predicted by geometrical optics. The focused spot size on the surface of the wafer depends on the wavelength of the laser light and the numerical aperture of the objective by

$$\varnothing = \frac{0.88\lambda}{NA} \quad . \qquad (1)$$

A detailed description of this phenomenon and its consequences for the lateral spatial resolution, both in ordinary microscopy and micro-Raman spectroscopy, is given in [22], along with suggestions for improvement. Here we are more concerned about the properties of the focused light along the z-axis, although we should be aware of the fact that our resolution in the xy-plane is limited by eq. (1), and will turn out to be the limiting factor in a lot of real measurements.
We have to distinguish between a focused beam with a uniform intensity distribution and a focused Gaussian beam. The uniform in intensity distributed beam focuses at the position predicted by standard geometrical optics to a diffraction limited spot. The beam will decrease in diameter when approaching the focal position like a cone, until it reaches the width described in eq. (1). Then, it will stay like this, until we come to the position at which the beam again becomes larger in diameter than the diffraction limited spot.
Gaussian intensity distributed beams behave completely different when being focused. For example, with a waist (smallest beam diameter) at the focal position of a single lens, for a *uniform* distributed beam the rays on the other side of the lens will all run parallel to each other. The second focal plane will then be somewhere at infinity, see fig. 2. *Gaussian* beams however, will have a secondary waist at the focal point on the right side.

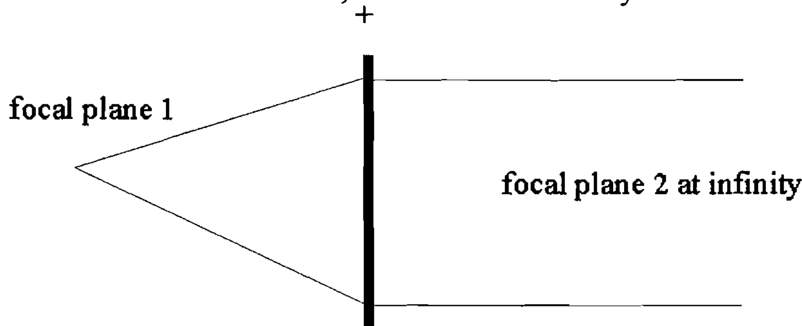

Behavior of a uniform intensity distributed beam

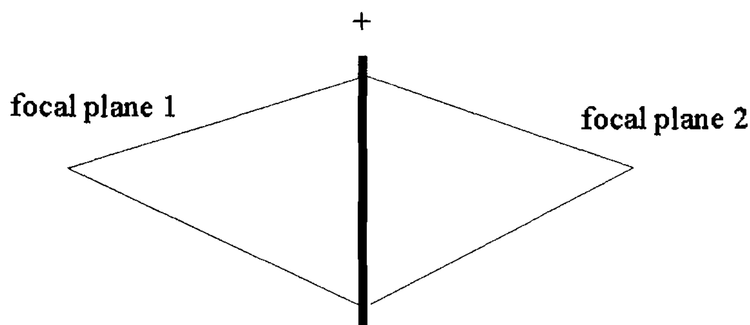

Behavior of a Gaussian intensity distributed beam

Fig. 2 Behavior of focused beams

The exact behavior of the beam passing a complete optical system does not concern us here, the interested reader can find a very useful calculation method in [20]. Depending on the part of the laser beam screened by pinholes etc. , the beam can behave as described in the uniform intensity distributed or Gaussian intensity distributed case. Here we are mainly interested in how a beam can be described when it is being focused by a positive lens, and we do only investigate the mathematics of the beam once it has passed the surface of the last lens. Self [20] supplies us with the necessary formulae.

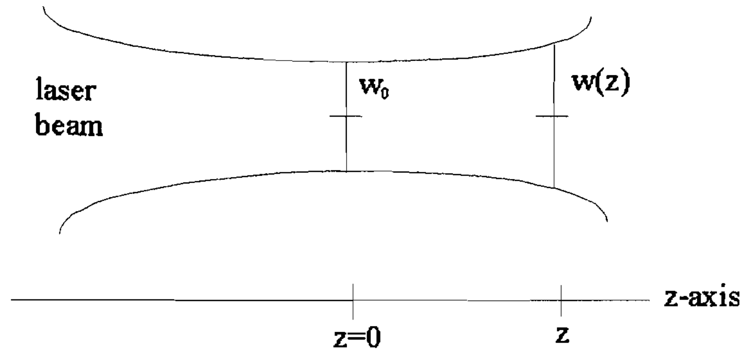

Fig. 3. Definition of beam waist

In this case our beam can be described in the xy-plane as

$$I(r,z) = I(0)e^{-2\left(\frac{r}{w(z)}\right)^2} \quad \text{, where}$$

$$w(z) = w_0\sqrt{1+\left(\frac{z}{z_R}\right)^2} \qquad (2)$$

is the dependence of the beam radius on the position at the z-axis, defined as the distance from the middle of the beam to the point where the intensity has dropped to $1/e^2$ of its intensity in the middle of the beam. The Rayleigh range

$$z_R = \left(\frac{\pi w_0}{\lambda}\right)$$

describes the rate at which the laser beam diverges , with w_0 the radius of the beam at the waist. It is the distance needed for the waist to grow to √2 of its minimum size. By expression (2) is stated that when we move the position of the beam waist, for example by changing the position of our lens, the beam diameter will be the smallest for one position, so in that case we can have the highest intensity on our detector from fig 1 if we put it at the same position as the waist. The intensity decreases when we move out of focus.

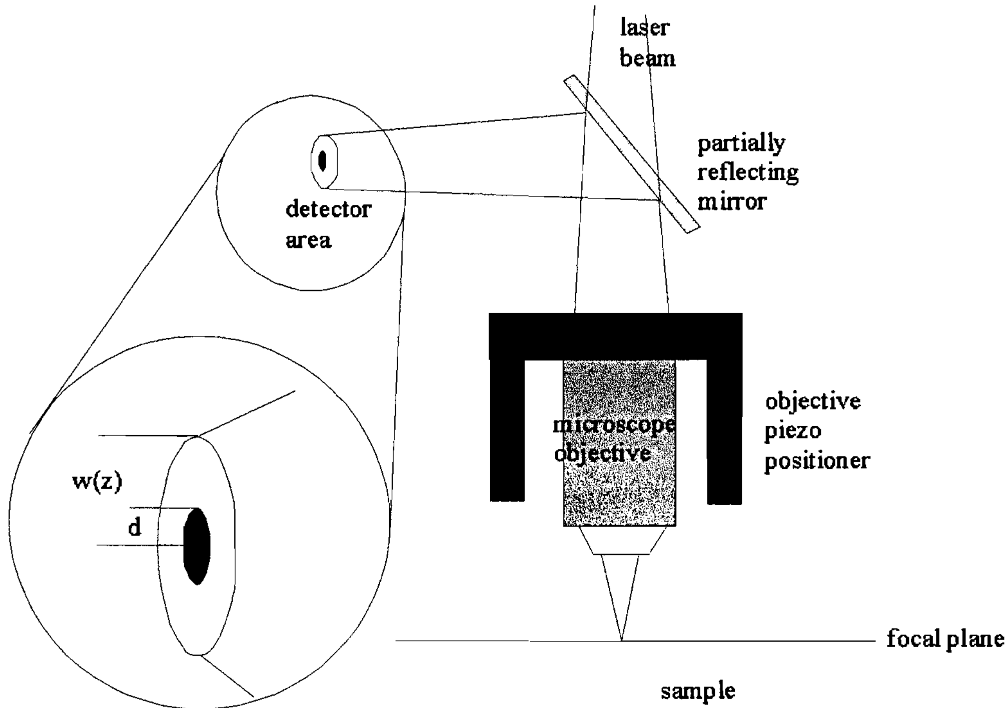

Fig 4. Height detection system

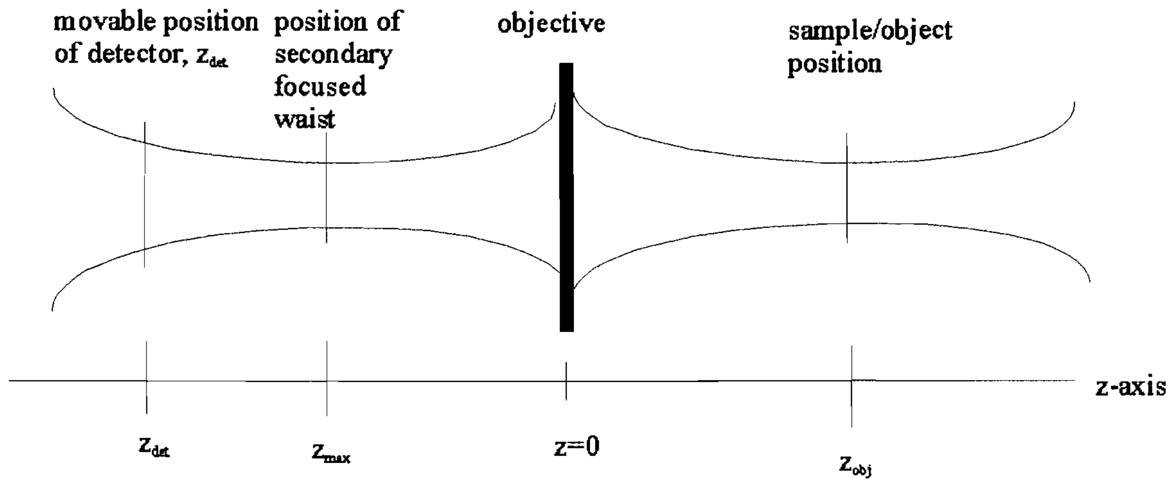

Fig. 5. Modeling of the height detection system

§4.4 Detector calculations and the z-axis intensity distribution

The elementary height detection system is depicted in fig. 4 and its model in fig. 5. The detector is a photodetector, with a radius d and an area πd^2. If z_{max} is the position of the secondary waist at the detector side of the objective, then the area on the detector illuminated by the laser beam is

$$\pi w^2(z) = \pi w_0^2 \left[1 + \left(\frac{\lambda(z - z_{max})}{\pi w_0^2} \right)^2 \right] \qquad (3).$$

Only the part falling inside the detector area is collected, so the intensity signal from the detector will look like

$$I(z) = \frac{I_{max} d^2}{w^2(z)} = \frac{I_{max} d^2}{w_0^2 \left[1 + \left(\frac{\lambda(z - z_{max})}{\pi w_0^2} \right)^2 \right]}.$$

For simplicity in future calculations, we will take some constants together and obtain

$$I(z) = \frac{a}{b + (z - c)^2} \,,$$

a Lorentzian function with

$$a = \frac{I_{max} d^2 w_0^2 \pi^2}{\lambda^2} \,,$$

$$b = \frac{w_0^4 \pi^2}{\lambda^2} \text{ , and}$$

$$c = z_{max} .$$

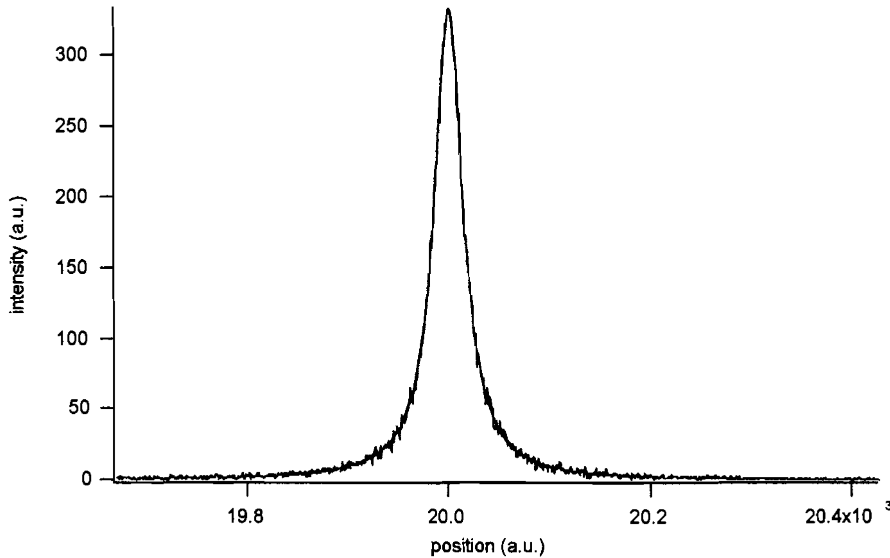

Fig. 6. Computer generated Lorenz intensity distribution with Gaussian noise.

The intensity is expected to vary like the computer generated curve in fig. 6 if we change the position of the sample on which we are focussing. This is only true if the detector is smaller than the smallest waist diameter. If the detector is larger, the complete beam will hit the detector, even if it is not yet completely focussed. The main part of the curve will not change, but the top will have a “clipped” like flatness. For now, we accept the necessity to have a detector collecting surface smaller than the beam waist. We can always achieve this by obstructing part of the collecting surface with a screen with a pinhole in it. The derivation holds only if the *detector* is moved through the focal plane so the sample to objective distance z_{obj} does not change. In our actual measurement setup, it will turn out that it is easier to move the objective, because then the same equipment can be used as a micro-Raman spectrometer auto-focus system. In that case, if the change in objective distance to the sample is linear, the resulting change in focal plane at the detector side is not linear.
We approximate the objective by a single positive lens. For a uniform in intensity distributed ray, we can use the standard lens equation from the geometrical optics approximation.

$$\frac{1}{z_{\max}}+\frac{1}{z_{obj}}=\frac{1}{f} \qquad \text{or} \qquad z_{\max}=\frac{z_{obj}f}{z_{obj}-f}.$$

If we insert the thus found z_{max} in eq. (3), we obtain the intensity as function of the objective to sample distance z_{obj}. In this case our z_{det} , the position of the detector, is not necessarily the position of maximum intensity z_{max} , so we call it z_{det} explicitly.

$$I(z_{obj}) = \frac{a}{b + \left(z_{\det} - \frac{z_{obj} f}{z_{obj} - f}\right)^2}$$

This will be the intensity distribution we will achieve when we move the objective through the focal plane and record the intensity with the photodetector.
For a real laser beam, the geometrical optics lens formula can not be applied. Self [20] again has our necessary equation, in this case the modified Gaussian lens formula for laser beams with a Gaussian intensity distribution.

$$\frac{1}{z_{obj} + \frac{z_R^2}{z_{obj} - f}} + \frac{1}{z_{\max}} = \frac{1}{f} \quad \text{or} \quad z_{\max} = f\left(1 + \frac{\frac{z_{obj}}{f} - 1}{\left[\frac{z_{obj}}{f} - 1\right]^2 + \left[\frac{z_R}{f}\right]^2}\right).$$

If we again insert the equation for z_{max} as z_{det}, as we did for the geometrical case, we find for our intensity

$$I(z_{obj}) = \frac{a}{b + \left(z_{\det} - f\left[1 + \frac{\frac{z_{obj}}{f} - 1}{\left(\frac{z_{obj}}{f} - 1\right)^2 + \left(\frac{z_R}{f}\right)^2}\right]\right)^2}.$$

Because this is the relation valid for our measurement setup, we can calculate differences in z_{obj} from our intensity distribution when moving the objective en hence make a height map of our sample. The actual behavior can be somewhere between the uniform and the Gaussian approximation due to screening of part of the laser beam with pinholes.

§4.5 Statistics of the z-axis intensity distribution

The uncertainty in the calculated focal plane position, and hence our resolution, depends on the noise present in the measured intensity. The main contribution to the noise in this intensity is the fact that the objective position accuracy is limited. The objective is positioned by a piezo transducer (PIFOC), and its position can be controlled by applying a voltage to the piezo. Unfortunately, there is always noise present in the output of a power amp stage, so the position of the objective will vary along with that noise. This varying position will influence the measured intensity, and so the intensity will be varying with the noise in the output to the piezo. Also, the output of the D/A-converter generating the positioning voltage is discrete, and so we have to consider a quantization error, but this error can be made very small by using a lot of bits to define small distance

differences. Perhaps the worst source of noise are vibrations in the system (induced by the laser cooling water flow, etc.), which can slightly defocus the whole microscope in a random way. This introduces another position noise term, which can seriously degrade the overall performance. The detection electronics will also add some noise, but we expect this to be not much, due to the high signal levels involved. What will then be the uncertainty in our height measurement? This depends on the error in the measured position of our objective.

We have seen in §4 that the intensity distribution along the z-axis is given by:

$$I(z) = \frac{a}{b + (z - z_{\max})^2} \qquad (4)$$

When we incorporate a term to describe the uncertainty in the actual position of the objective, this will look like:

$$I(z) = \frac{a}{b + (\bar{z} + \delta z - z_{\max})^2}$$

Now we assume that the position of the objective is normally distributed with the mean at the position we would like the objective to be (the output of the D/A-converter), and a standard deviation which accounts for the deviation from this mean value.

From fig. 7 we see that the uncertainty in the position of the detector will not add equally much noise to the intensity for all positions. Note that here we are changing the position of the detector, and not of the objective. This simplifies the calculations and still gives us some useful insight in the error sources in our system.

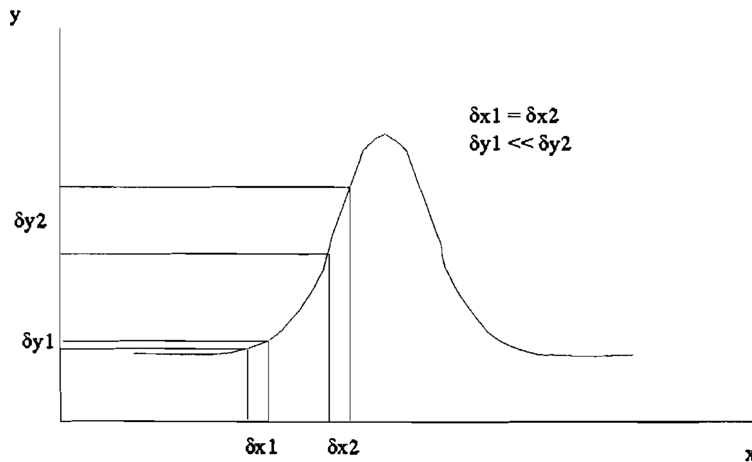

Fig 7. The uncertainty in x will give different uncertainties in y depending on the slope of the function

Where the intensity stays almost the same when moving the detector a little, inaccuracy in the objective position is not likely to give a large error. However, if the intensity changes rapidly when moving the detector or objective, as is the case when we approach the focal plane, a little change in the position of the detector will cause a large error in the intensity. If we call the standard deviation in the position of the objective σ_z and the standard deviation in the intensity σ_I we find, using equation (4) and fig 7. , the standard deviation in the intensity as a function of z, in which we assume that the standard deviation in z is not large compared to the actual z value:

$$\sigma_I = \left|\frac{\partial I}{\partial z}\right| \sigma_z = \left|\frac{-a(2z-2c)}{(b+(z-c)^2)^2}\right| \sigma_z \qquad (5)$$

When we fit the intensity curve by χ^2 minimization, we will find a calculated position of the focal plane which is much more accurate than simply taking the measured position at which the intensity was the highest. What we see from this equation is that σ_I (and hence our noise) becomes the largest when z-c approaches 0, in other words: near our focal plane. The further we move from the focal plane, the smaller the amount of noise in our measured intensity. Also if we are really close to the focal plane, we are on the top of the Lorenz function, and our intensity will not vary much with distance. Here the noise should be not high also, but only for a very small region. This is made clear in fig. 8.

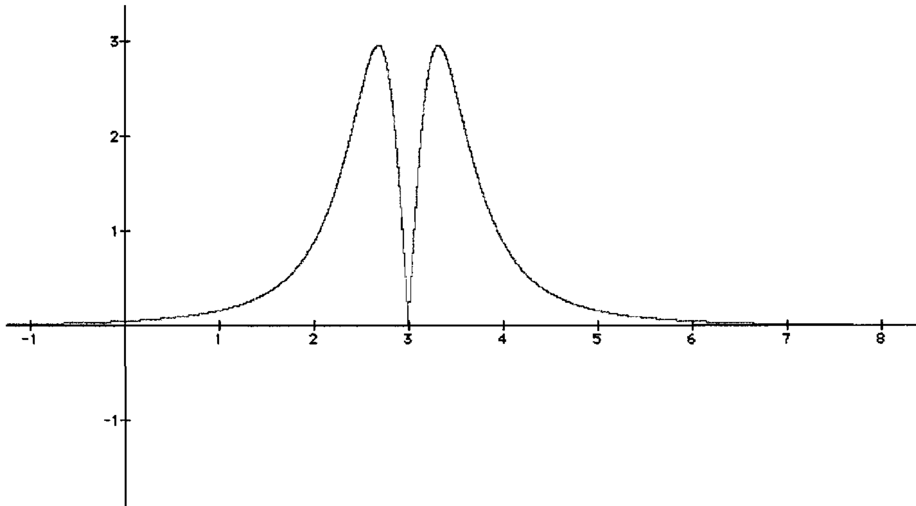

Fig. 8 Graphical representation of (5) : horizontal σ_z , vertical σ_I, arbitrary units .

We can define the output of the D/A converter as the mean of z, which can take values from 0 to $2^{16} - 1$ (16 bit) due to the step-like voltage output of a D/A-converter en hence the quantisized movements of our objective. For each position of the objective n (which can take values from 0 to 2^{16}-1), the value of σ_{In} will be different due to (5).
The χ^2 statistic as function of the fit parameters and the actual data is given by:

$$\chi^2 = \sum_{n=0}^{2^{16}-1}\left(\frac{I_n - I(\bar{z}_n;a,b,c)}{\sigma_{I_n}}\right)^2$$

Minimization of χ^2 is equivalent to finding the parameter values for which the first derivative of χ^2 with respect to the parameters is zero:

$$\frac{\partial\chi^2_{\min}}{\partial a} = \sum_{n=0}^{2^{16}-1}\left(\frac{I_n - I(\bar{z}_n)}{\sigma_n^2}\right)\left(\frac{\partial I(\bar{z}_n;a,b,c)}{\partial a}\right) = 0,$$

$$\frac{\partial\chi^2_{\min}}{\partial b} = \sum_{n=0}^{2^{16}-1}\left(\frac{I_n - I(\bar{z}_n)}{\sigma_n^2}\right)\left(\frac{\partial I(\bar{z}_n;a,b,c)}{\partial b}\right) = 0, \text{ and}$$

$$\frac{\partial\chi^2_{\min}}{\partial c} = \sum_{n=0}^{2^{16}-1}\left(\frac{I_n - I(\bar{z}_n)}{\sigma_n^2}\right)\left(\frac{\partial I(\bar{z}_n;a,b,c)}{\partial c}\right) = 0.$$

Unfortunately, these equations can only be solved if the derivatives are linear in their parameters, although they may be nonlinear in x [19]. In this case they are not, and the only way to find the distribution in the position of the focal plane, is by numerically evaluating the parameters for different input data. This can be done by Monte Carlo simulation, but because of the large uncertainties in our input quantities, for example the effect of vibrations of the microscope on our objective to sample distance, this is not really useful if we want to know the uncertainties in our measurements. We can, however, say that they will be much smaller than the uncertainty in the actual position of the objective due to the large averaging effect of our curve fit, and do a lot of measurements with the system to estimate them. This means that by using the curve-fitting algorithm, we have circumvented the diffraction limit along the z-axis!

CHAPTER FIVE
Description of the height measurement system

§5.1 Introduction and system setup

The curve-fitting height measurement system contains the components in fig 1. We have a short wavelength laser (Argon, 457.9 nm), which gives a smaller focused spot, and hence more spatial resolution in the xy-plane, than a large wavelength laser (typically in the 600 nm range for a He-Ne laser). This laser is focused through a high precision optical microscope. The computer controls the movement of the sample in the x and y direction, so that the focused spot can reach all positions on the sample. The microscope objective can be moved along the z-axis to change the focal plane position. Ten percent of the light reflected from the sample through a beamsplitter is focused again on a photodetector. The signal from the photodetector goes to the measurement electronics, which will be covered in more detail in §3.

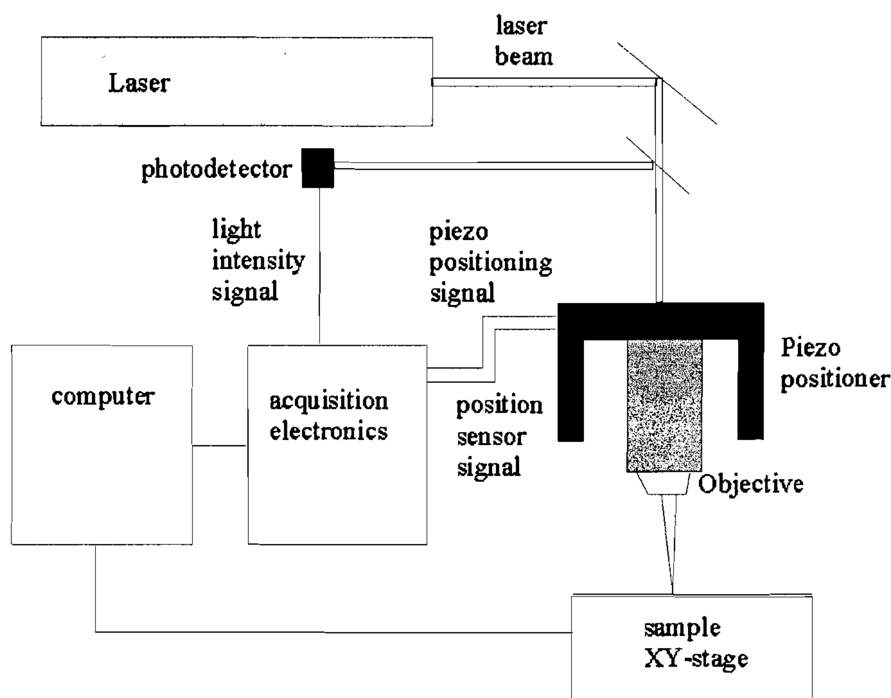

Fig 1. Height measurement setup.

The objective is scanned along the z-axis for each measurement point in the xy-plane, collecting at each point an intensity distribution as a function of the focus position. By curve fitting this distribution for each point, the exact position of the focal plane, and hence the height of the surface on that point, can be calculated.

§5.2 Requirements

A couple of different profilometers do exist, most of them based on a kind of interference principle. They offer good performance, but are very expensive, and their technology cannot be easily adapted to already existing measurement systems like the Dilor micro-Raman system at IMEC.

Even more important was the fact that the Dilor micro-Raman system lacked a really good auto-focus system, which is very important when scanning a large area or using very high numerical aperture objectives with a very small depth of focus, like a 100x objective, an oil immersion lens or a solid immersion lens (SIL). For this purpose it was needed that the auto-focus system could communicate with existing Dilor micro-Raman acquisition software.

It would be also very useful if it were an "open" acquisition system, in which new measurement techniques could be easily implemented by some small changes. It that way the same electronics could be used for height measurements, auto-focus purposes, LIVA, TIVA, OBIC, OBIRCH and even Kerr Rotation based Current Measurement. Only some readily available extra equipment, like a constant current source, would be needed for each failure analysis technique.

§5.3 The piezo transducer

To perform the very precise movements of the objective required by the height measurement application, an actuator was needed with a very high accuracy. To perform very small movements with a microscope objective, in the nanometer range, special "microscope objective nano positioners" (PIFOC) can be obtained. They consist of a couple of piezo-electrically active crystals, with the possibility of an optional built in position sensor. The one we chose was a microscope objective positioner with a maximum translation of 350 micron. This large maximum translation was chosen so that the topography of larger structures, such as solder bumps on an IC , could be investigated.

The sensor is very important because a piezo crystal exhibits peculiar behavior when voltages are applied to it. Not only does it change shape (which is what we would like a position actuator to do), but it suffers from hysteresis and creep. The hysteresis manifests itself as the fact that the same voltage does not necessarily mean that the objective is in the same position (fig 2.). This might be corrected for by always starting at the same position when focusing, but this does not prevent the other effect from occurring, the creep. This means that after a step-function-like voltage change is applied, the piezo does not immediately reach its final value. It will take several minutes before the piezo stops moving significantly (fig. 3.). For that reason, we cannot position the piezo by just applying a voltage to it, but we have to incorporate a control system. This is probably the reason why the Dilor auto-focus system did not work really well. They used almost the same actuator, but had no control loop to verify whether the position of the microscope objective was the same as they wanted it to be. Fig. 2. shows the behavior of a device similar to ours but with a translation maximum of 35 microns.

Physik Instrumente (PI) provides sophisticated control electronics for this purpose, so an OEM version, to be built in with the microcontroller electronics, was obtained from them. This control electronics contains also the power amp stage, for the 100V the piezo

needs. The input signal is just a voltage, which is converted to a position of the objective. There were some problems with this module due to oscillations, but after recalibration at PI, the module performed reasonable, although here is still room for improvement.

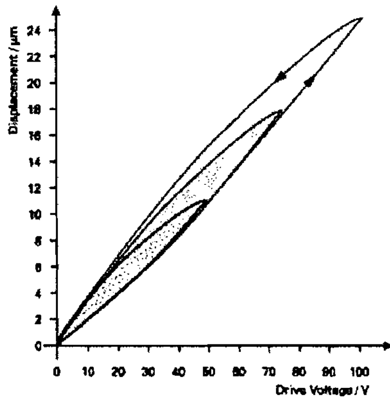

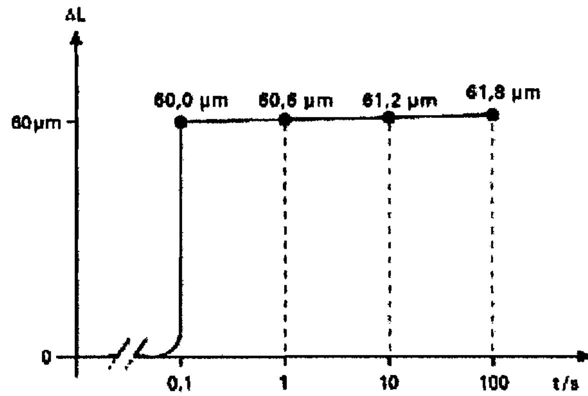

Fig 2. Hysteresis Fig 3. Creep

Figures taken from http://www.physikinstrumente.com (Physik Instrumente)

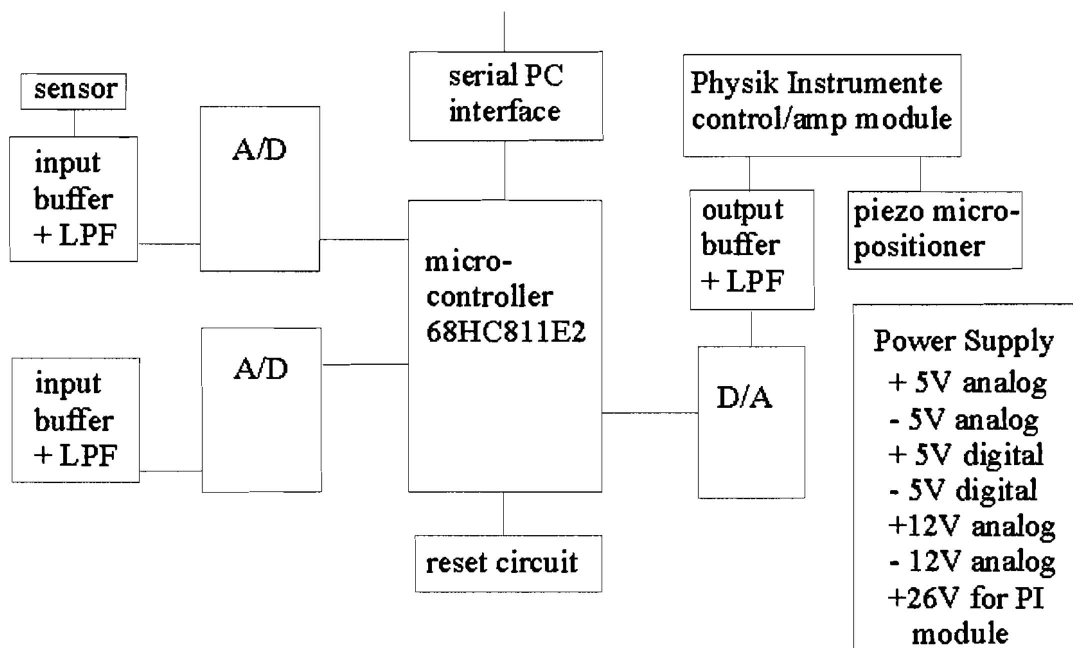

Fig. 4. Simplified schematic of the acquisition electronics

§5.4 Description of the electronics

A simplified schematic of the height measurement electronics is given in fig. 4. The heart of the system is a Motorola MC68HC811E2 microcontroller, with 2kB of EEPROM, 256 bytes of RAM, a serial communications interface (RS232) for use with a host computer, and a serial peripherial interface (SPI) for communication with other devices, such as A/D converters [7]. Two 16 bit A/D converters are used to sample the intensity of the

detector in the microscope, and a 16 bit D/A converter is coupled to the power amp with control loop which generates the voltage for the microscope objective piezo positioner (PIFOC). A RS232 serial interface is used for communication with the host PC. In fig.5 a detailed schematic is given, the print layout is given in appendix A.

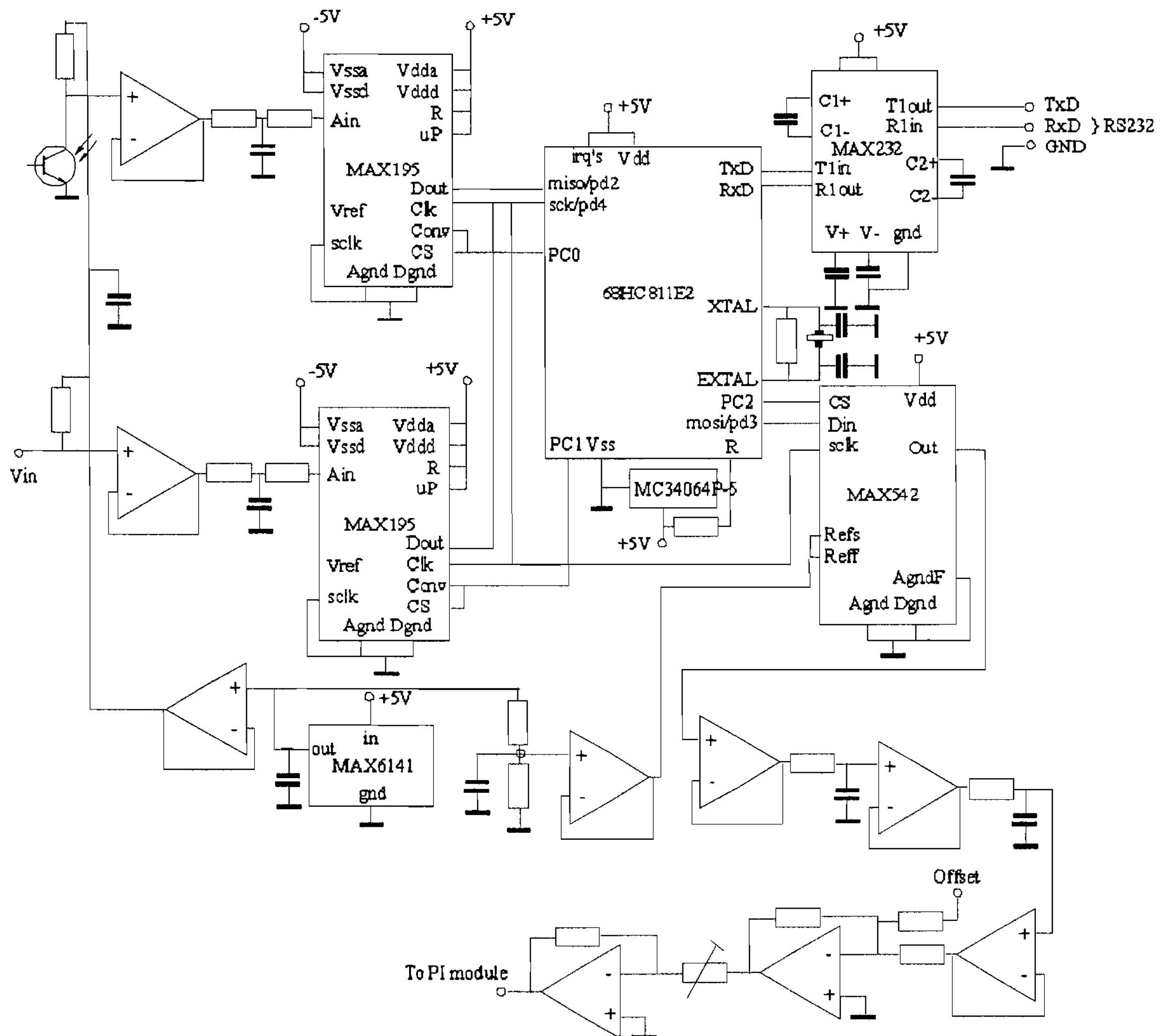

Fig. 5. Schematic of the micro-controller electronics

§5.5 Brief introduction to the software

The micro-controller can operate in five modes. The mode is selected by the program running on the host PC. In mode '1' , the module performs a height scan at one position on the sample. The objective is moved over the full 350 micron and all the intensity values associated with the position are sent to the host PC using the serial cable and stored in a file called inty001.me1. At the next position on the sample inty002.me1 is generated, etc. The user can specify the scan area on the host computer to 0.1 micron precision (in our system the smallest possible movements of the XY-stage). In mode '2', only the intensity data near the peak position are sent to the host computer to save time ("adaptive-focus" area scan). Mode '3' is the Raman auto-focus mode. Running this

mode causes the module to focus to the focal plane once, as described in chapter 6. For mode '4', the photodetector is not used. This is the LIVA/TIVA imaging mode (chapter 7). The acquisition module monitors the voltage across a constant current source, and sends all the data to the host PC. In mode '5' , the LIVA/TIVA image is collected, but with the second A/D converter the intensity of the reflected laser light is monitored at the same time. This generates two images: a LIVA/TIVA image, and a kind of "photograph" of the scanned area with the same resolution as the LIVA/TIVA image.
On the host PC these modes are selected, and a mode select code is sent to the micro-controller module. The host PC also sends commands to move the XY-stage. The XY-stage part of the software was derived from the Dilor Raman spectroscope acquisition software.

§5.6 Measurement results

§5.6.1 Performance of the A/D and D/A

One of the first things to check after assembly was the performance of the sensor read-in A/D-converter and the piezo positioning voltage D/A-converter. To perform the test, the output of the D/A was fed back to the input of the A/D and a ramp voltage was programmed. The result is shown in fig. 6. The linearity is very good. By zooming in on the measured ramp voltage, it was found that the noise present obscures about two bits. This noise is probably due to coupling of digital noise to the analog circuit. This was to be expected because the precautions to prevent this only consisted of different supply voltages for the analog and the digital part. Maybe a ground plane would improve matters somewhat, but for our application 14 bit resolution is perfectly adequate.

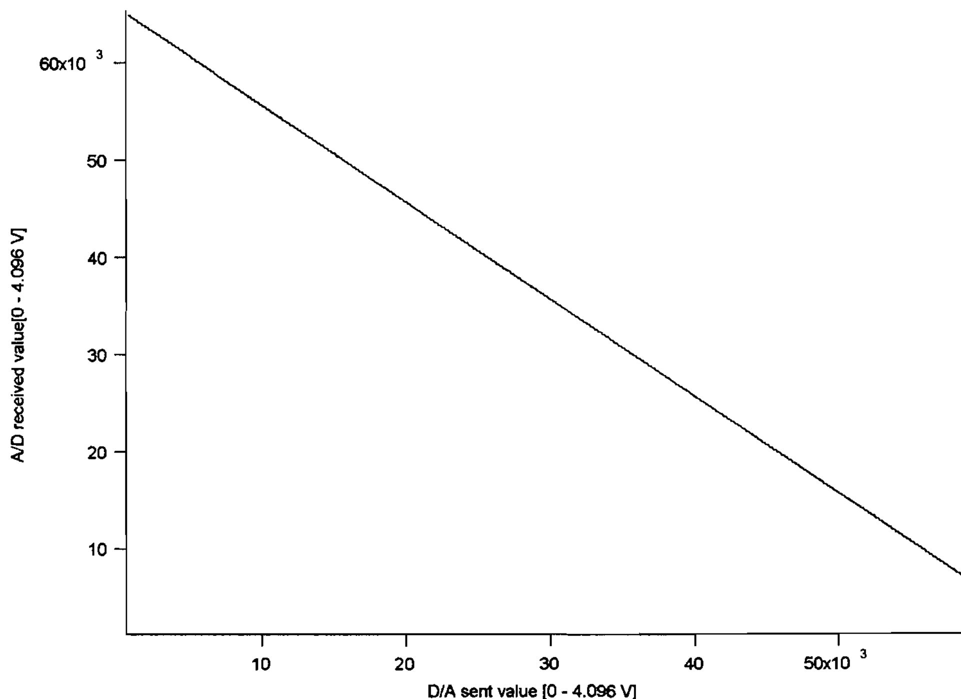

Fig. 6. A/D and D/A converter performance.

§5.6.2 The PI control system

To correct for the piezo hysterese and creep, a LVDT position sensor and PI-control electronics (second order control loop) is provided by Physik Instrumente. They cannot however optimize the control system beforehand for every objective mass. In our case the positioner burst into oscillation as soon as is was turned on with the objective mounted. After changing the P and the I term of the controller it became stable, but the position noise was about four micron, which was much too large to be useful. The step response in closed and open loop (fig. 6 and fig 7) were recorded, and then the controller was sent back to PI for recalibration with an optimization for an objective mass of 125 g. Note the very high position noise in the closed loop case. Once this calibration had been done, the positioner behaved reasonable, but some little objective movement remains visible.

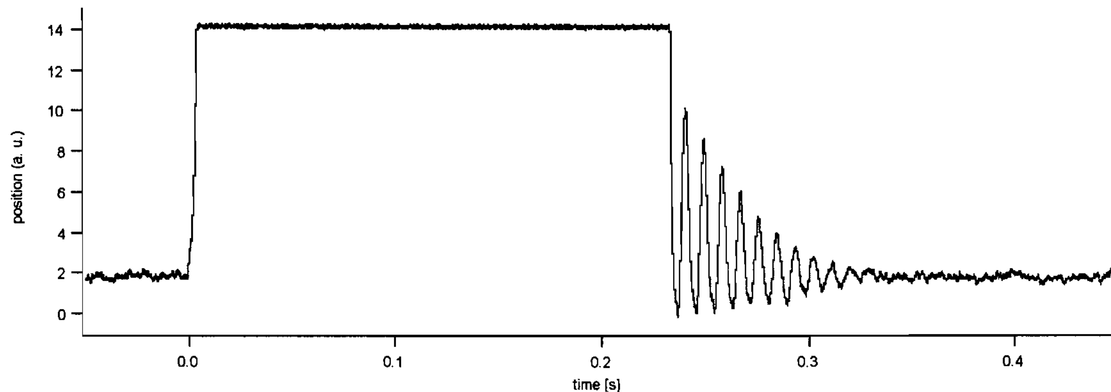

Fig 7. Open loop step response of the not yet calibrated piezo with objective.

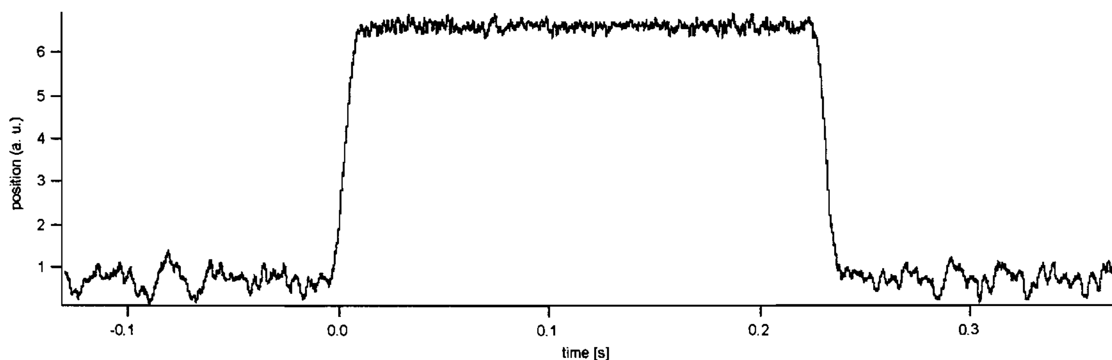

Fig 8. Closed loop step response with very high position noise.

§5.6.3 Intensity profile

A lot of intensity noise near the exact focal plane is introduced by the noise in the position of the objective as described in chapter 4. Also, a very precise outlining of the laser beam pinhole is required, otherwise we see the predicted "clipped-like" flatness, also surrounded by noise. Because the 50x long distance objective has a larger area in which the objective is almost in focus (due to the smaller NA of 0.55 instead of 0.95 than the 100x lens) we see that its intensity distribution is a little broader than that of the 100x normal objective. On the other hand, it is easier for the curve fitting algorithm to find the peak in the intensity, and so the focal plane, when less noise is present and the curve more closely resembles a Lorenz function, as is the case with the 50x LD objective,

where the intensity rises and falls less sharply. We see that the 100x lens curve suffers from the "clipped" top as described in chapter 4.

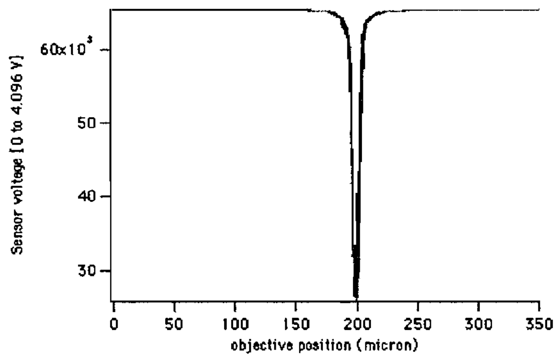

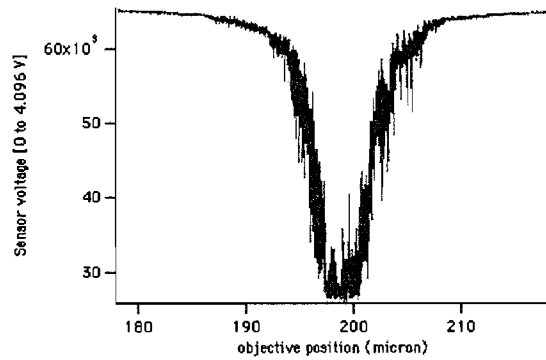

Fig. 9. 50x LD Intensity vs objective position

Fig 10. Close-up of fig. 9.

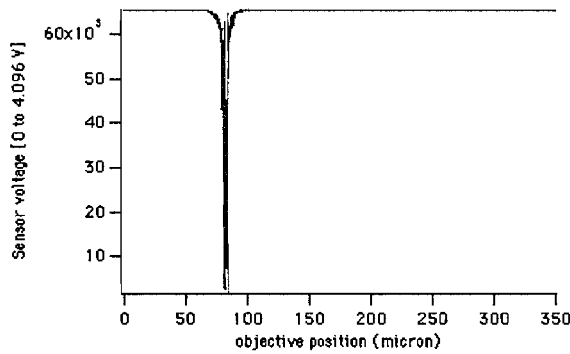

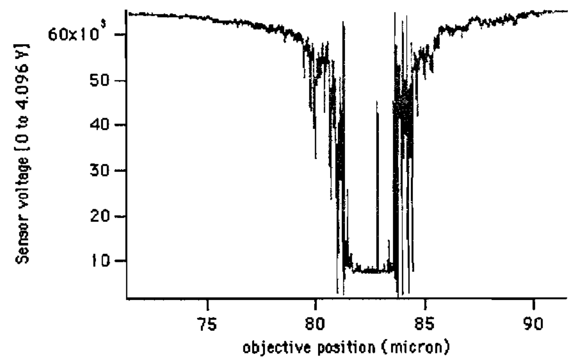

Fig. 11 100x Intensity vs objective position

Fig. 12. Close-up of fig. 11.

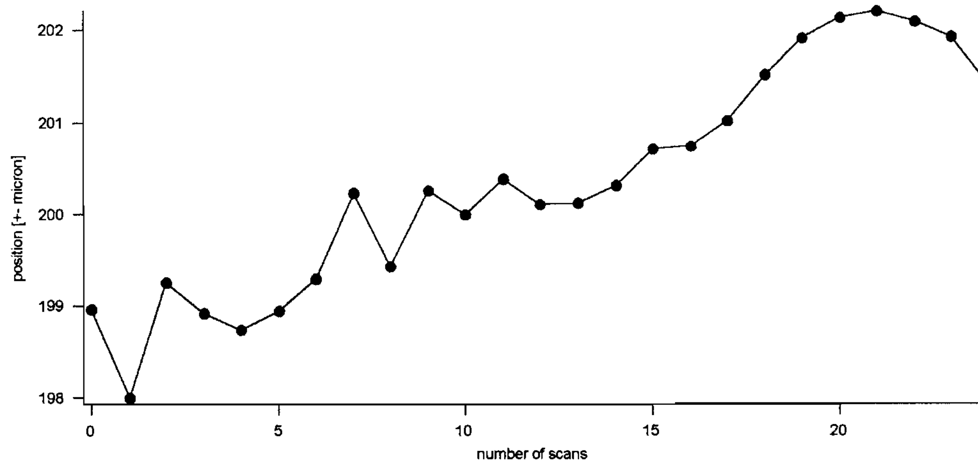

Fig 13. Drift of sample to objective distance.

§5.6.4Repeatability of the height measurement
In fig. 13 we see the result of a couple of slowly taken height scans at one position (taken in a couple of hours). The peak intensity found by curve fitting drifts over a couple of microns, most likely due to room temperature variations: the distance between sample and objective simply becomes larger or smaller with temperature changes. This effect has already been known for a long time [12]. Another source of error, which is hopefully smaller than the previous mentioned one, might be the hysteresis and drift of the piezo control electronics of PI.
The precise distance changes are not yet really known. As we saw in chapter 4, they depend on whether we use the Gaussian intensity distributed laser beam approximation, or the uniform distribution. The only way to calibrate the height measurement is to use a sample with known height differences.

§5.7 Conclusions and future work
One of the main problems at the moment when performing height scans is the long acquisition time. It takes a lot of time to send all the measured intensity values to the host computer using a serial cable. Because of these long acquisition times, there is plenty of time for the temperature to change or for the electronics to drift from their initial value. The long acquisition times are also impractical when one wants to measure the height profile of a complete area.
To improve this, first the crystal frequency of the micro-controller board has to be chosen in such a way that it supports higher baud rates in the communication with the PC. Second, we don't need all the intensities of all the 65536 positions over the full 350 microns the piezo positioner can move. We only need to collect the data near the intensity peak. This could be performed by a kind of "adaptive focus" algorithm. It detects the first changes in intensity higher than a certain threshold, sends the associated position, and starts sending data for about 20 micron or so. This takes much less time than to send the same data for 350 micron. Even within those 20 micron we might be able to get along with less than sixteen bit resolution (187 points per micron), if our application does not need such a high resolution, or if it turns out that the drift in the electronics is much larger than that. Also, if the PI module turns out to be the main error source, there are some signals available on the PI module connector to build a custom control loop for the piezo.
If all these possibilities are combined, the resulting improvement in acquisition time will enable us to perform topography scans over a complete area with high resolution. Theoretically the achievable resolution only depends on the specifications of our positioner and the number of bits, and, most important, not on the depth of focus of our objective. For that reason, we can circumvent the diffraction resolution limit of the x and y axes when we measure along the z axis. This means that if we can precisely control the movements of our positioner, the achievable resolution can be easily less than a single nanometer, despite the diffraction limit of half a micron!
Of course a curve fitting distance measurement system can be used well outside its current context of measuring the height of micro-electronic structures. It can also be used as the sensor in a precision positioning device, or to measure macroscopic distances with high precision.

CAPTER SIX
The micro-Raman auto-focus system

§6.1 Description of the micro-Raman system

The micro-Raman system used at IMEC contains a high power 457.9 to 514 nm Argon laser, a computer controlled XY-stage, a microscope, a foremonochromator and spectrograph, and CCD camera with a computer interface (fig. 2, chapter one). The light is focused on the sample with the microscope, and the Raman signal generated at the sample, as well as the reflected laser light, is collected by the same microscope for further processing. The Raman signal can be used for measurements concerning mechanical stress in the sample, its composition, crystallinity and local temperature. The reflected laser light can be used in the same way as with the curve-fitting height measurement to focus the microscope automatically.

§6.2 Application of the auto-focus system

The use of an auto-focus system for micro-Raman spectroscopy brings with it some very special problems not encountered in ordinary auto-focus systems [2], [9]. Most important, the Raman signal is not always collected at the surface, but sometimes a little bit underneath. This means that the best focus is not always achieved when the surface is in focus. So a program part has to be built in, to add a specific offset to the found best focus position. Second, we do not have a complete image, on which we can perform all kinds of computations (image processing), but only one spot, which can be smaller or larger depending on the position of the objective, and at the position we want to focus, its size remains almost constant for about two micron (depth of focus of the objective, depends on the NA). The time needed to perform the auto-focus algorithm has to be short, not more than a couple of seconds, because common micro-Raman spectroscopy experiments already take a lot of time without auto-focus possibilities. This is not really a problem though, because we only have to focus to a 250 nm accuracy. So we have to find an optimum between speed and accuracy.

§6.3 Description of the auto-focus algorithm

It takes about five seconds to scan across the complete 350 micron z-translation the positioner is capable of. So it is not desirable to do more than one scan for the auto-focus algorithm. Because we know the high intensity distribution to be approximately 2 micron wide for both the 50x long distance and 100x objective (50x a little more, but it has a larger depth of focus too), we can just look at the first position at which our intensity is below a predefined threshold. The intensity function is very steep there, so it is not really crude to use this specific position, and this position is for that reason not much affected by the chosen threshold. After we have found this position, we add one micron, and we are in the middle of the intensity distribution, and hence in our focal plane! It could hardly be expected that such a simple approach could ever give good results. It was intended as the first step in a more complex algorithm (and more time consuming too), but it turned out to work really well.

§6.4 Results

In fig. 1 we see the intensity of a Raman signal when we focus just once on a Si sample, and do a couple of measurements very near to each other with this setting of the equipment. We see that a slight drift out of focus causes the intensity to decrease a little, but that is not much. A histogram of the intensities is given in fig. 2., so we can actually see the intensity distribution across the measurements. Now we do the same measurement with our auto-focus system focusing again for every measurement point (fig. 3. and 4.). Note that the result with auto-focus is a little *better*. The intensity of the auto-focus measurement is also a little better, so it can be assumed that the initial focusing by hand was already worse than the auto-focus focusing. The intensity distribution with auto-focus is smaller than the distribution without auto-focus, suggesting that the focusing is more reliable and predictable than when focusing by hand.

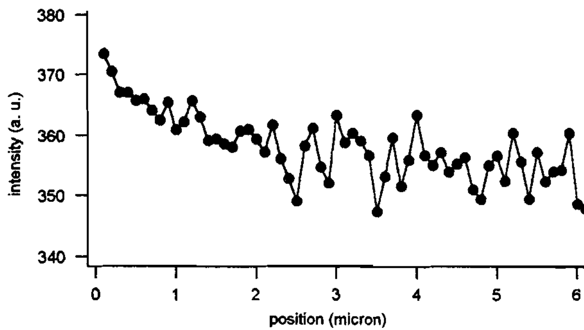

Fig. 1. Intensity without auto-focus

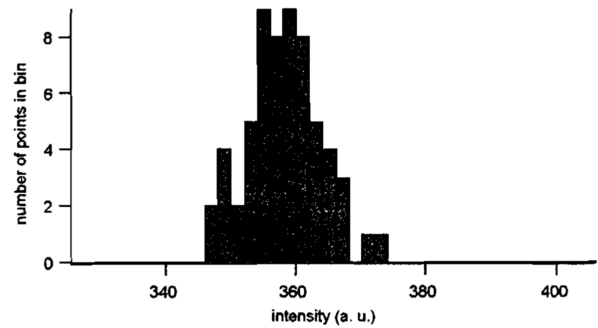

Fig. 2 Histogram of intensity without auto-focus

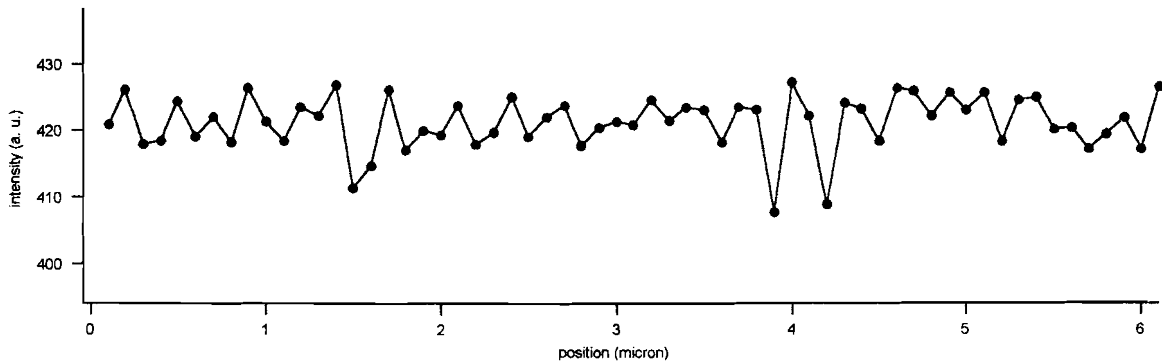

Fig. 3. Intensity with auto-focus

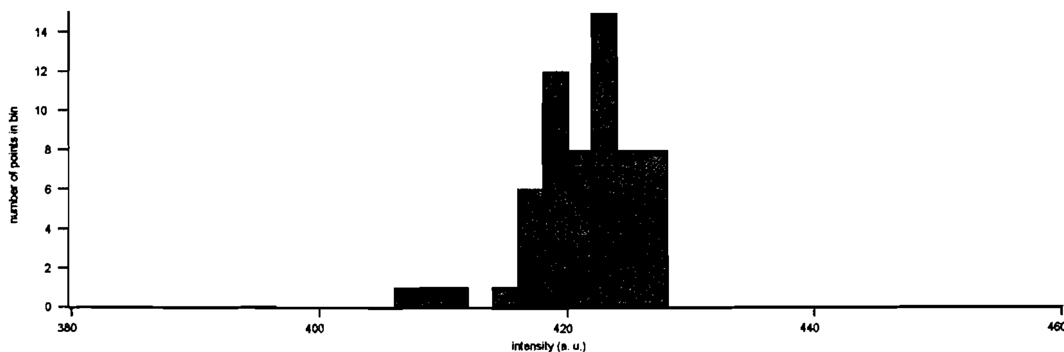

Fig. 4 Histogram of intensity with auto-focus

The real advantage of an auto-focus measurement setup is of course not the focusing to a single focal plane, but to measure samples with large height differences. For the test a wafer with Silicon On Insulator (SOI) structures on it was taken. If we cut such a structure it looks like in fig. 5. The height differences between the surface of the Si islands and the top surface of the Si substrate are 3.4 micron, which is too much for a normal 100x objective, because its depth of field is only 1 micron. In fig. 6. the Raman signal intensity is given of the measurement without the auto-focus system. The Raman signal intensity is high if the laser spot is probing the high silicon on the oxide, but it almost vanishes due to defocus, when we reach the underlying silicon. The auto-focus module will focus both on the top and bottom silicon, and hence the intensity of the Raman signal should stay almost constant.
Fig. 8 shows the Raman intensity in the auto-focus experiment. The intensity is the same for both the top and the bottom silicon, which means that both of them are in focus. Only at the edges the result is less good. The transition takes 1.5 to 2 microns, while we can see from the experiment without auto-focus, that the edges are much sharper and can be investigated with 1 micron resolution.

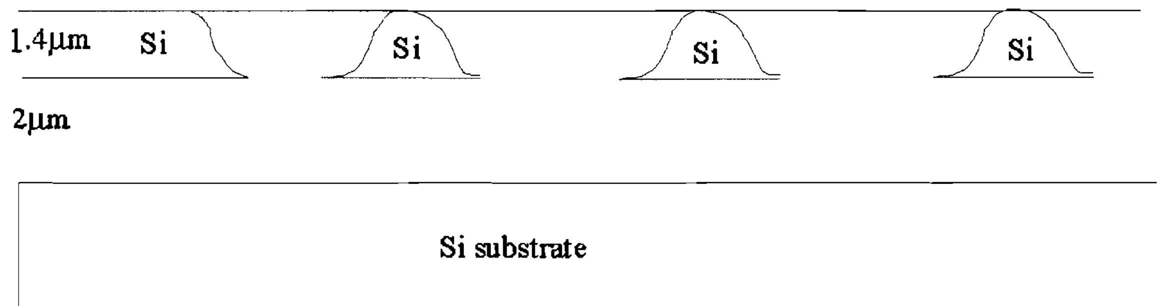

Fig. 5. Silicon On Insulator (recessed oxide)

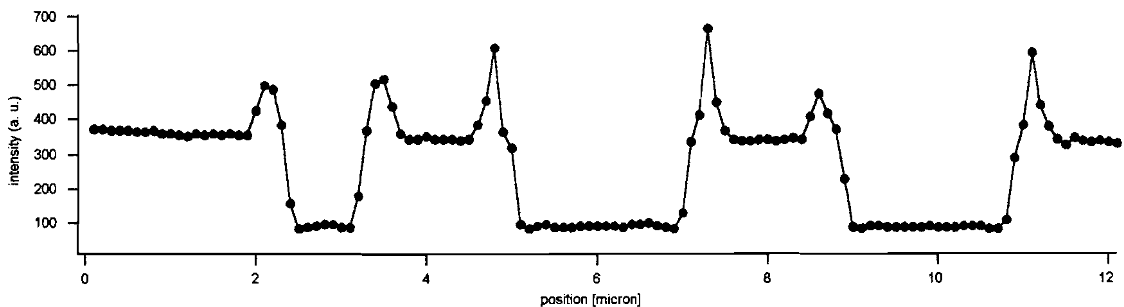

Fig. 6. Measurement on the SOI corresponding to fig. 5 without auto-focus, 100x objective, intensity of Raman signal.

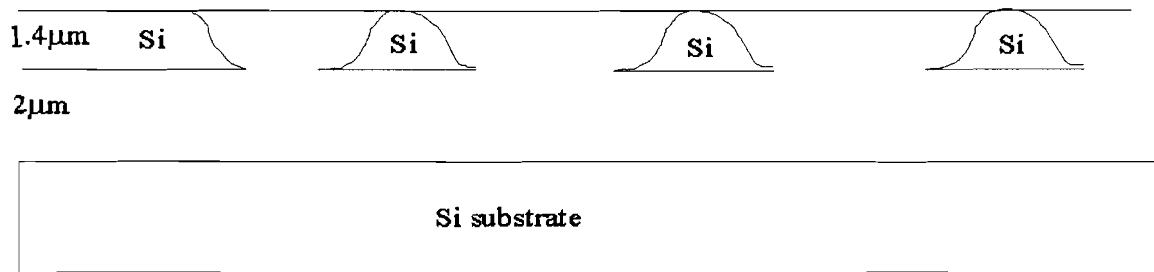

Fig. 7. SOI structure for the measurement of fig. 8.

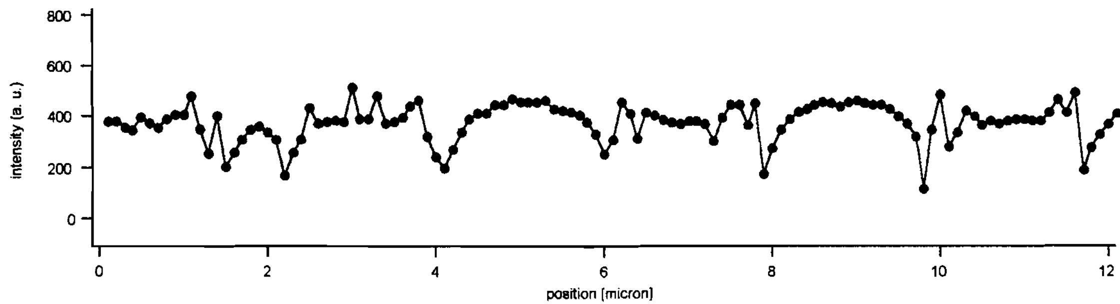

Fig. 8. Measurement on SOI corresponding to fig. 7 with auto-focus, Raman intensity.

We can also have a look at the peak position shift of the Raman signal (chapter one), to investigate the stress distribution in our sample. We know from chapter one that 1 cm^{-1} shift corresponds with approximately $2 \cdot 10^{-9}\sigma$ [Pa]. From fig. 9 and 10 we see that, although the intensity in the non-auto-focus experiment is much lower, we have obtained almost the same Raman peak position shift.

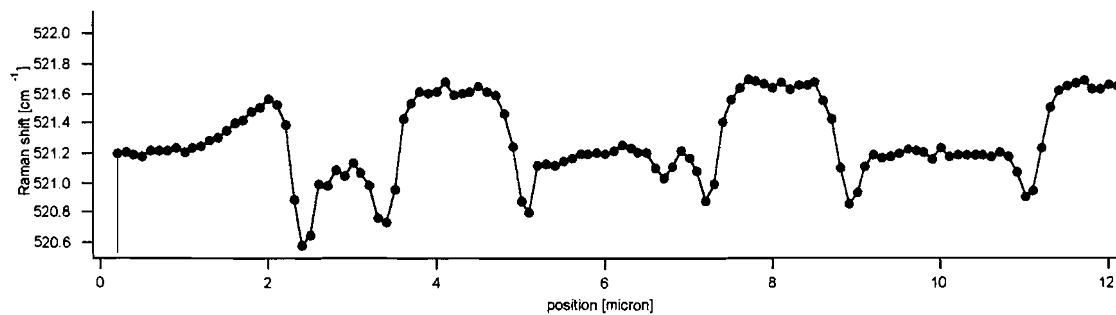

Fig. 9 Raman shift of the SOI measurement without autofocus.

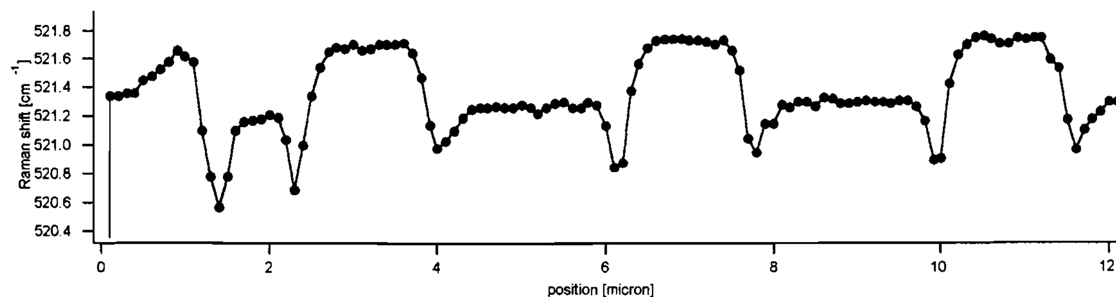

Fig. 10. Measurement on SOI with auto-focus, 100x objective, Raman shift.

§6.5 Conclusions and future improvements

For a lot of applications the auto-focus module as it is now is very useful and performs as one would expect from such a device. It focuses as good as when manually focusing or even a little better, also with large height differences.
At the moment there are a couple of drawbacks though. First, it performs not so good near edges in structures. This is certainly a disadvantage, because these are the most interesting positions if we are interested in mechanical stress.
Furthermore, if the intensity of the reflected laser light is very low, as when crossing the edges of an SOI structure, sometimes the intensity does not even reach the threshold of the auto-focus. In that case it starts looking for the focal plane forever, or until we turn up the laser power and reach the intensity threshold. Of course that is not the way it has to be, because Raman experiments often take several hours, in which we don't want to sit next to an auto-focus module waiting until it crashes again. Also, the increased power will affect our measurement. For this reason, the threshold should be made variable: if a full scan does not find the intensity peak, lower the threshold automatically and try it again.
Near edges the part of the distribution with high intensity along the z-axis becomes broader. Signal is acquired from the bottom and top of the edge, and so it can easily become a couple of microns wide. By measuring the width of this distribution and positioning the objective in the middle, we might get an even better focus than is achieved now. Both improvements are only needed to do high resolution scans near edges. In all other experiments the auto-focus module behaves very well.
When using an objective with a small depth of focus, e.g. a 100x objective, vibrations of the auto-focus piezo are visible. This is due to the control electronics, and cannot be solved unless it is decided to build a custom control loop. Even in that case it cannot be assured that this phenomenon will completely disappear.

CHAPTER SEVEN
Expanding the measurement electronics to LIVA

§7.1 Carrier generation by light incident on a semiconductor

When light is incident on a semiconductor, the photons will be absorbed, or they can propagate through the material, depending on the wavelength (and hence the energy per photon) of the light and the bandgap of the semiconductor material. If the energy of the photons is smaller than the bandgap energy of the semiconductor, they will not be readily absorbed, and can travel quite a distance through the semiconductor: the material appears to be transparent at this particular wavelength. When the photons have an energy larger than the bandgap energy, they can generate electron-hole pairs and will be absorbed. Stated formally, this means that

$$h\nu = \frac{hc}{\lambda} > E_{gap}$$

for photons to be absorbed by the semiconductor. The intensity of the photon flux decreases exponentially, when propagating through the material, with an absorption coefficient α [cm^{-1}] [14]. This means, when x is the distance traveled in the material and $I_{\nu 0}$ [Energy/cm^2] is the incident flux, that

$$I_\nu(x) = I_{\nu 0} e^{-\alpha x}.$$

Because of the generation of carriers by short wavelength photons, the absorption coefficient α is a strong function of this wavelength. For Light Induced Voltage Alteration (LIVA) it is important that these carriers are generated, so the wavelength should be in the region in which the absorption coefficient of silicon is large (short wavelengths). If we assume that one absorbed photon generates one electron-hole pair, the generation rate g' is

$$g' = \frac{\alpha I_\nu(x)}{h\nu} [\# / cm^3].$$

We see that the number of generated photons in a volume is linearly dependant on the incident flux, and will be the strongest near the surface for high α.

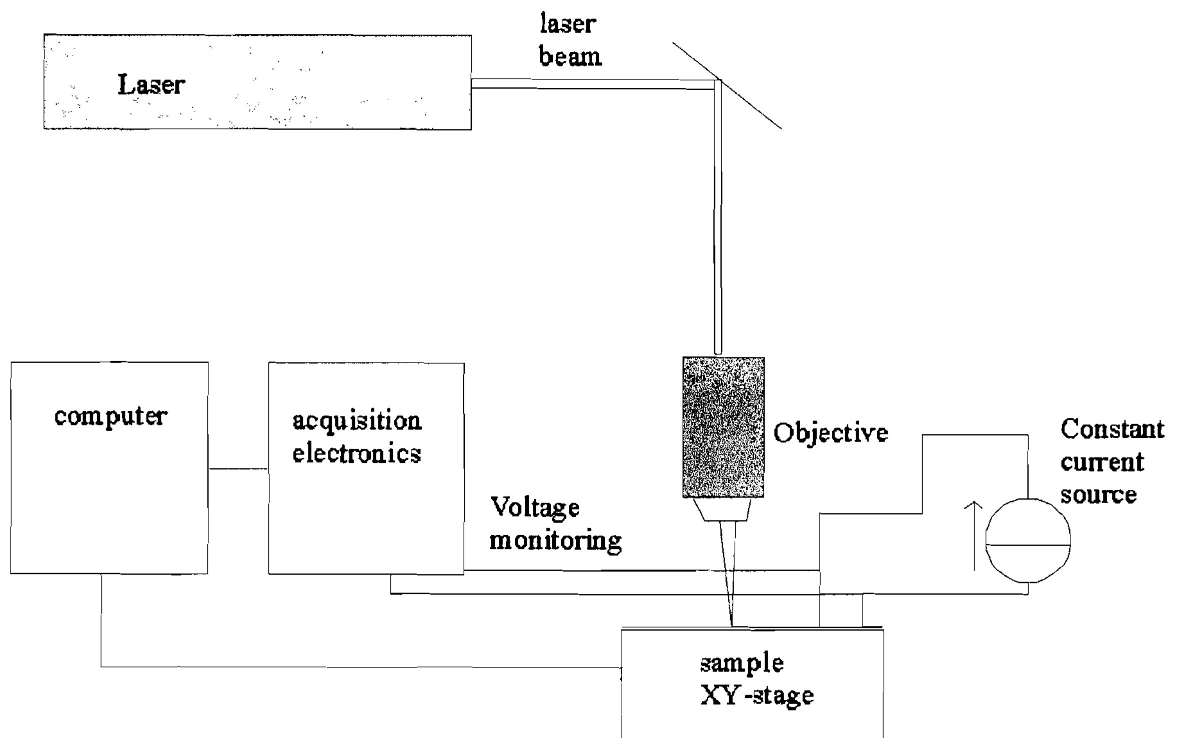

Fig. 1. LIVA imaging measurement setup

§7.2The LIVA imaging principle

The theoretical measurement setup is depicted in fig. 1. We see the Argon laser (457.9 nm) which beam is focused through a microscope onto the sample. The sample is a complete IC, connected in such a way that it is not biased, but its supply voltage can be accurately measured. The power is applied to the IC using a constant current source. The movements of the sample underneath the microscope objective and the voltage measurements are controlled by a personal computer.

When the photons are generated by the laser light near the interface between differently doped regions in the IC, the charge is separated by the same built-in potential effect as in the pn-diode. The laser beam is scanned across the sample, and the voltage fluctuations across the terminals of the constant current source are measured. In this way a LIVA signal (either an increase or decrease of the IC power demand) is observed [3]. The amplitude of the LIVA signal is also dependent on the "logic state" of the transistor, because there is a greater difference between source and drain voltage when the transistor is not conducting.

The current changes are small in the laser spot region, but these little changes will be amplified by the succeeding transistor stages. The observed LIVA signals from localized defects on integrated circuits such as opens are often much larger than the signals of non-defective ICs.

§7.3Implementation in the micro-Raman setup

With the control electronics already covered in chapter three, it is easy to do the LIVA measurements. We connect the constant current source to the IC and monitor its supply voltage with the acquisition electronics. Then we scan a laser beam focused by the microscope objective across the IC.

§7.4 Measurement software

The first LIVA experiments were using the Dilor Raman software to move the XY-stage. This turned out to be very slow, because the minimum time needed to collect one Raman spectrum is about three seconds, even if the Raman signal is collected only for 0.01 second. For area scans the acquisition time soon becomes prohibitive, so a special piece of software was programmed to do the whole measurement on its own. The measurement is now performed 15 times faster. The acquisition software performs the following tasks:

1. Selection of scan type (height measurement/LIVA)
2. Calibration of XY stage and COM ports
3. User input for scan area an step size (0.1 μm minimum step)
4. Moving the XY stage during the scan
5. Collecting the intensity or LIVA data at each position
6. Writing the data to a user specified file

It turned out that the communication between the module and the host PC was not completely reliable, so a very simple error correction was programmed as well. Every byte is sent thrice, so if two out of three are the same, this was the correct byte. With this correction code, everything works very well and without errors in the communication between the electronics and the computer.
The LIVA imaging is still not as fast as would be desirable for complete die investigation, but it is expected that the improvements given by the future work topics will be enough to make it a very useful tool in failure analysis.

§7.5 Measurement results

LIVA is very useful to find opens in a defective IC. To test the system, a metal line leading to a couple of transistors was cut using the focused ion beam technique (FIB). In the first picture (fig. 1.) we see the cut in the left top corner (arrow). The second one (fig. 2.) shows the complete area of which a LIVA scan was taken.
We see some transistors which are all connected with their gates to a single metal line (the one we cut). In fig. 3. we see the LIVA signal. This was taken with a 50 mW laser output power at

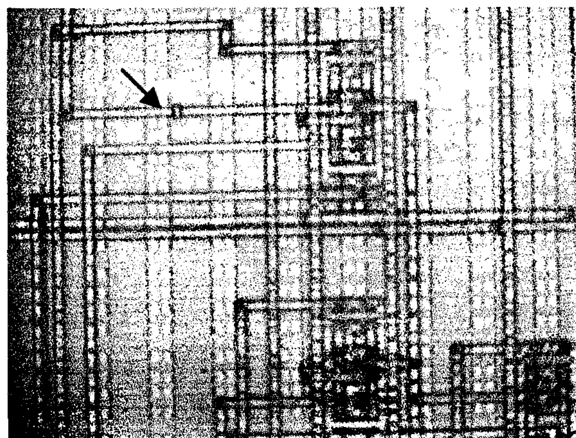

Fig. 1 FIB cut in left top corner

457.9 nm (blue light) with a 10x objective and one micron difference between each sample point. We see that the some regions of the transistors near one of the power busses (the long straight lines running from the top to the bottom of the picture) give a very large LIVA signal. This is due to the changes the carriers make in the working point of the transistors. This working point can change considerably, because the floating gate does not impose a well-defined state upon the transistors as a real logic level would. Fig. 4. shows the same region on a chip where the line was not cut. The transistors are still visible, but the signal is much weaker. They are hardly visible above the background intensity on the rest of the IC (note that the surface without active areas gives the same color on both images).

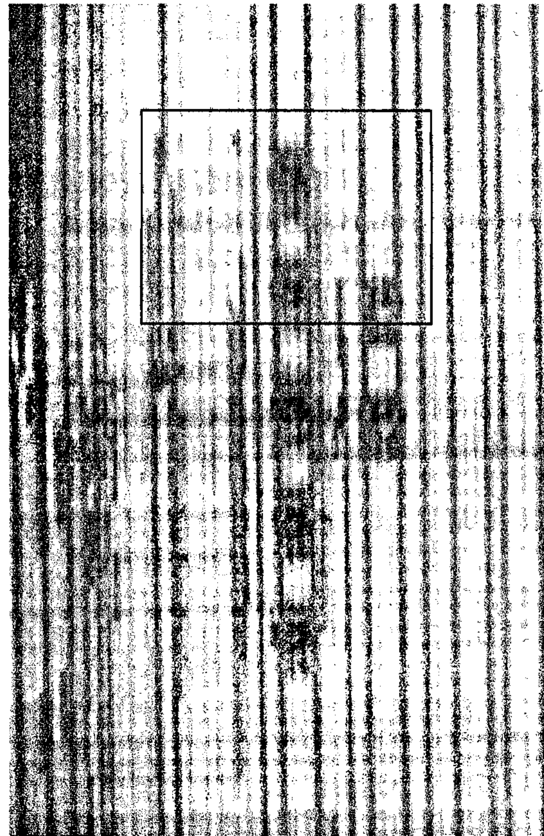

Fig. 2. Photograph of the transistors connected to the defect gate line. The square depicts the area in fig 1.

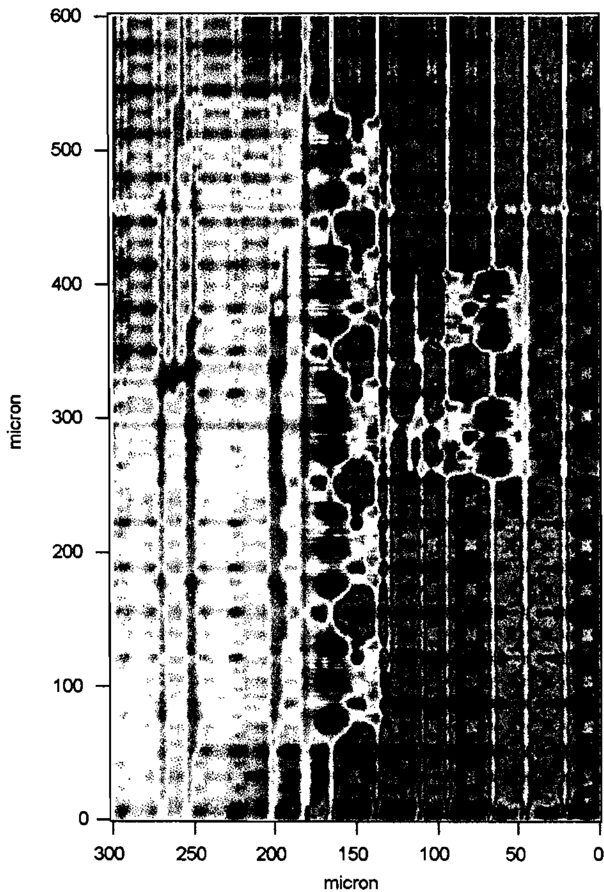

Fig. 3 Transistors with defect gate line

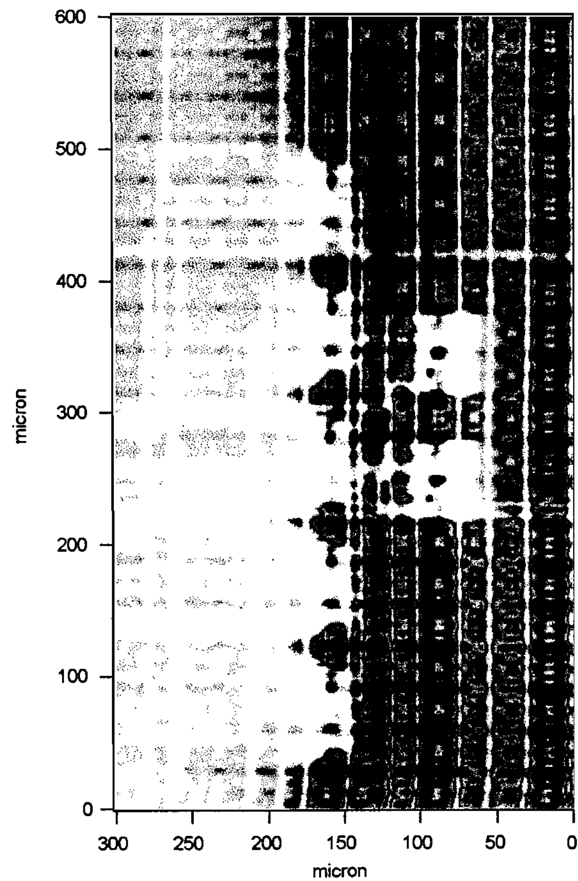

Fig. 4 Transistors with a good gate line

In fig. 5., 6. and 7., we see a close-up of some of the transistors. Fig 5 is a photograph, fig 6. shows the IC with the defect. In fig. 7 the colors have been adjusted so we can now see that the same structures are visible as in fig. 6. Note that the contrast is still less, because the maximum signal intensity is much lower with non-defect structures. In [21] it is claimed that the active regions of a transistor which give a LIVA signal are state-dependant. This means, that if the logic state of a transistor in fig. 6 or 7 would change, we would be able to see the difference!

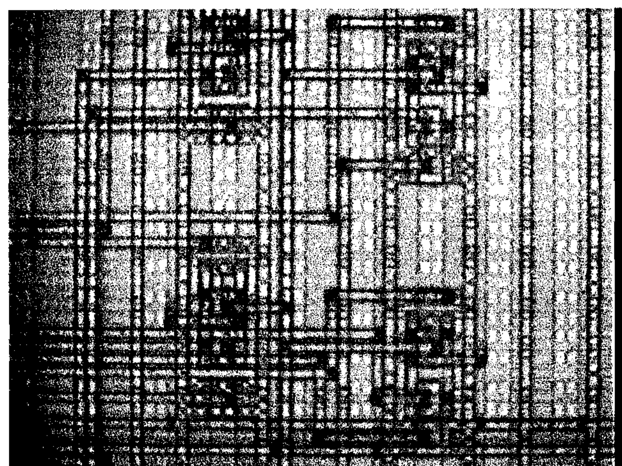

Fig. 5 Close-up of transistors, defect gate line

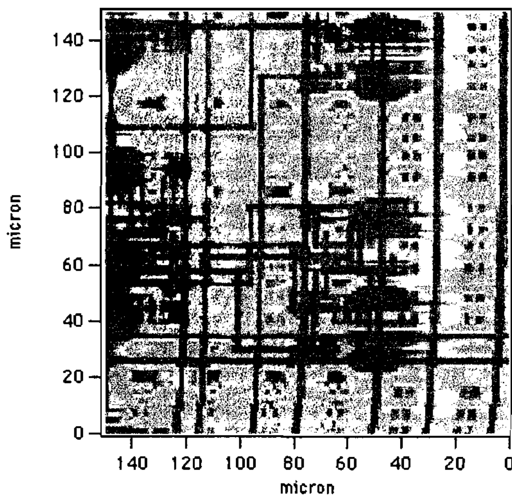

Fig. 6. Close-up of transistors on defect IC

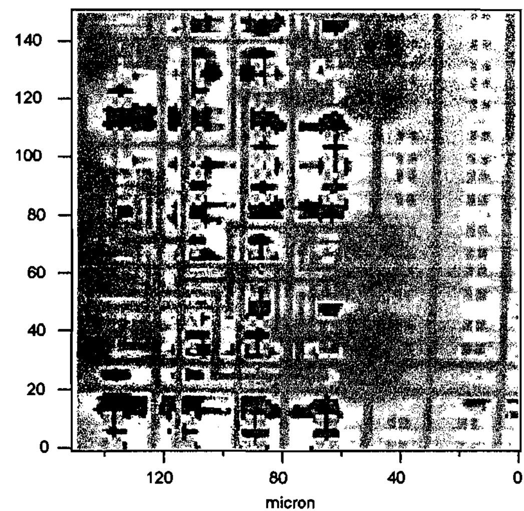

Fig. 7. Close-up of non-defective structures

On the right we see in fig. 8 (arrow) another line which was cut using a FIB. Note that the line itself is almost invisible in the LIVA image (fig. 9.), but that the connected transistor gives a large LIVA signal. Here we see a disadvantage of LIVA. We know in which region the fault is expected to be, but we don't know its exact location. With TIVA (chapter 9) it is possible to see such a floating line itself running to a gate. Disadvantage of TIVA is the much lower signal levels involved, and the need of an IR-laser. In fig. 10 and 11, we find a particle on top of the IC in the memory array. No large LIVA signals are associated with this particle, so it is expected to be on top of the passivation layer, and not to influence the IC behavior. We see only the screening of the part of the circuitry underneath the particle, but the intensity of the whole image was low, so no defects detectable with LIVA are present.

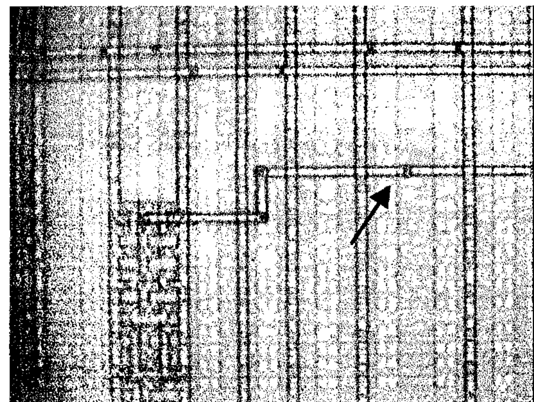

Fig. 8. Line cut with FIB

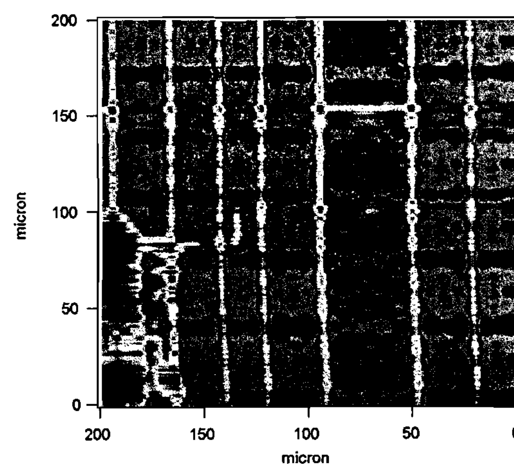

Fig 9. LIVA image: line is hardly visible

§7.6 Conclusions and future work

The modified micro-Raman spectroscopy

equipment can be used to do LIVA measurements with high spatial and voltage resolution. It has been shown that this LIVA system can detect the difference between transistors in a circuit with floating

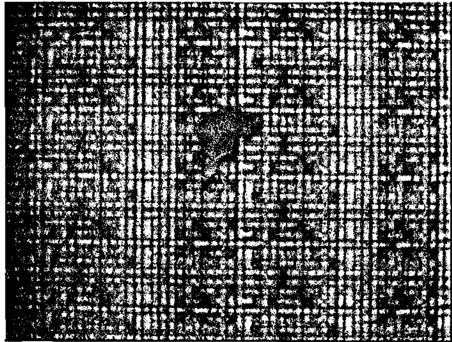

Fig 10. Particle in memory array

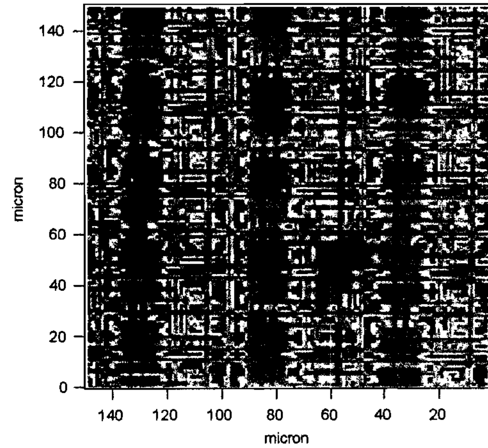

Fig. 11 Corresponding LIVA image

gates and the same transistors in a properly functioning circuit. The defective transistors generate a much larger LIVA signal than the normal circuitry, so they can be found by scanning the entire IC and defining a threshold level above which the intensity is marked as occurring due to a defect.
Due to the slow movements of the XY-stage scanning a complete IC takes too much time at present to be practical. At this moment every time the XY-stage is positioned, and afterwards one position is measured.
The first thing to change are the movements of the XY-stage. It is possible to let it move with constant speed and perform LIVA voltage position measurements in rapid succession. Also, the Raman system has the possibility to scan with a mirror and have the spot moving over the IC very fast. Maybe this option can be used as well.
The high LIVA signals can also be detected by a scan with a less high spatial resolution, followed by a precision scan over the smaller suspected area.

CHAPTER EIGHT
Image restoration – The spatial approach

§8.1 Introduction
The spatial resolution of the micro-Raman measurements is limited by the finite size of the probing laser spot. Everything present within the area illuminated by the spot is measured at the same time, so the line scan or image shows no undistorted detail smaller than the spot size. Although this seems unavoidable, there is more information in the image, because information about every detail in the image *is* collected. The problem is how to extract this information from the blurred image. The blurring is due to the intensity distribution of the spot, so, if we know exactly the properties of our probing spot, we can correct for these introduced faults by electronic (computational) means. This leads us to the field of image theory, and linear image operations in particular. In image theory, two-dimensional images are often used, but in micro-Raman spectroscopy line-scans are performed most of the time. For that reason we will look at the one-dimensional version of the problem. In the one of the last paragraphs the extension to a two-dimensional formulation applicable to real images is briefly looked upon.

§8.2 Convolution and the PSF
The point spread function (PSF) is the projection of a *point* on the object line to the image line (both described by an x-axis).
In our case, the point spread function is caused by diffraction, as already discussed in chapter four. This function is not depending on the position in the image line, so we can write:

$$PSF = h(x - x_1) = \frac{J_1(x - x_1)}{x - x_1} \approx e^{-(x-x_1)^2}$$

in which x_1 is the position of the center of the spot. It gives the response of the imaging device to one single point source. The intensity dE(x) along the image line is proportional to the impuls response function of the imaging system, $h(x\text{-}x_1)$, and some constants due to properties of the system, here omitted for clarity; see [8] for more details on the subject. $J_1(x)$ is the first order Bessel function of the first kind.
When we have not a single point, but an intensity profile I(X) along the object line, we have:

$$dE(x) = h(x - sX_1) \cdot I(X_1) dX_1 \ ,$$

with s a scaling factor depending on the geometry of the problem. Radiant energy is additive if it is incoherent, and although the laser light is coherent, the Raman signal is not. If we only look at the Raman signal, we can find the intensity distribution on the image line by integrating this expression on both sides. We obtain a convolution integral (by scaling the coordinates of the object for simplicity):

$$E(x) = \int_{\xi_{min}}^{\xi_{max}} h(x-\xi)I(\xi)d\xi = h(x) * I(x) \qquad (1)$$

We find that the intensity distribution E(x) along the image line is related to the original object intensity distribution by equation (1). When we know everything except for the intensity distribution of the object, we can also calculate it from (1).

§8.3 High emphasis filtering

In our *object line*, we take intensity samples at discrete positions, which we can regard as a vector $\mathbf{f}_n$. The PSF can also be regarded as a vector, denoted $\mathbf{h}_m$. If the line is long compared to the part at which the PSF has a significant value, we can take m << n.
The *collected vector at the image line* $\mathbf{g}_n$ is the discrete counterpart of convolution (1). We can perform a linear image operation on $\mathbf{g}_n$:

$$\mathbf{i}_n = \mathbf{M}_{n,n}\mathbf{g}_n ,$$

with **M** a n by n operation matrix, which assigns a value to each output vector component according to the input vector components and **i** the *calculated vector*. If this operation does not depend on the position of the component and it is linear, it is the discrete counterpart of the convolution.
For one component of the vector **i** we can write:

$$\mathbf{i}[q] = \mathbf{h}_{q,n}\mathbf{g}_n .$$

In this equation, $\mathbf{h}_{q,n}$ is the qth *row of the operation matrix*. So now we have a tool to do the inverse of the convolution which had taken place by converting the object to the image plane. We only have to find a matrix **M**, such that the original convolution (which can be written in the same way), is counteracted.

What is the shape of this matrix? We know that a particular point **g**[q] of the image is collected by the convolution:

$$\mathbf{g}[q] = \mathbf{h}_{q,n} * \mathbf{f}_n ,$$

in which $\mathbf{h}_{q,n}$ is the discrete PSF. This is basically a low-pass filter. The low frequency components in the image are left unchanged (they are much larger than the PSF), but the high frequency components, smaller than the point spread function, are attenuated, because they are smeared out over a couple of vector components. The complementary operation of the low-pass filter is a high-pass filter $\mathbf{1}-\mathbf{h}_{q,n}$, with **1** the vector which is zero everywhere except for position q, where it is unity.
It attenuates the low frequency components, but leaves the components smaller than the PSF unchanged. Our object consisted of both low-frequency and high-frequency components, so we want the low frequency components, which are still in the image to

remain the same, but we want the high frequency components to be amplified to such a level, that the imaging convolution is compensated. This is what we achieve when we combine the original image linearly with is high-pass filtered version, which is called high-emphasis:

$$\mathbf{h}_{high-emphasis} = \alpha \mathbf{1} + (1-\alpha)\mathbf{h}_{q,n} \qquad (1)$$

The amount of high emphasis applied is governed by the dimensionless constant α.When we perform such an operation for each component of the vector $\mathbf{g}_n$, we can regain our original object vector $\mathbf{f}_n$. We fill the matrix M with rows in which the peak of the PSF is moved one step for each succeeding row, like what happened in the original scan. When our model of the PSF is very accurate, much of the blurring caused by the PSF can be removed, but noise will obscure the very high frequency components, which were severely attenuated, so we can never get an exact replica of the object vector.

§8.4 Program description

The implementation of this image restoration algorithm in C is given in appendix B. The convolution operation is performed on each component of the image vector separately, so that no complete matrix M needs to be constructed. Furthermore, the PSF is only taken into account where its value is significant, so this vector is much less in dimension than the image vector is. The points near the edge of the line are not corrected: we would need the intensity of points which were not measured to do this. First we have to decide upon our PSF. It is assumed to be Gaussian, but we know from chapter one, that this is only an approximation. The spot size and the value for α can be given by the user of the program. The input image file is "igor.txt", the reconstructed output file is "recon.txt". A brief description is given in table 8.1.

TABLE 8.1 IMAGE RECONSTRUCTION PROGRAM
Declaration of variables
Declaration of arrays to stack the data
User input: Spot size and α
Calculate discrete PSF from spot size (Gaussian)
Read input file "igor.txt" and store in an array
Calculate high pass filtered image
Combine this image with the original according to $\alpha\mathbf{1} + (1-\alpha)\mathbf{h}_{\text{high-pass}}$
Print output to screen
Save restored image as "recon.txt"

§8.5 Results

The image restoration algorithm was used with data from a scan over a sample of silicon with $TiSi_2$ lines on it. The Si gives a peak in the Raman spectrum at 520 cm^{-1}, the $TiSi_2$ does not give any signal. From the transition from no Raman signal to maximum Raman signal the probing laser spot size can be calculated [21]. This is the same kind of

experiment as described in chapter 1, but with a sample with $TiSi_2$ lines instead of nitride lines. Two plots are given, one for a normal measurement with a 50x long distance microscope objective (fig. 1.), with and without image enhancement, and the other for a measurement with a special near-field lens, the solid immersion lens (SIL) in fig. 2. In both cases we see an improvement of the spot size, but for large values of α noise and the uncertainty in the real PSF slope give errors (in fig. 2 the intensity of the image enhanced violet line drops below zero!). For small values of α however, the resulting image is much better than without image restoration. Especially the result of the combination of the HSIL with the image restoration technique is quite impressive.

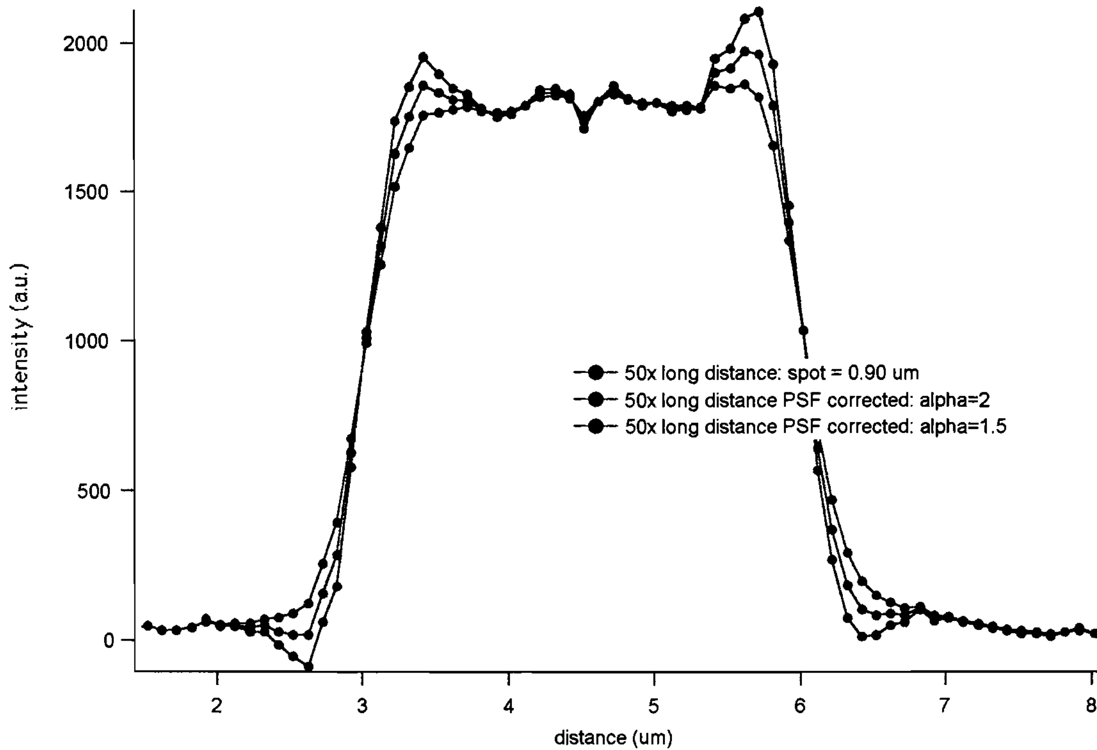

Fig. 1. Resolution enhanced scan over $TiSi_2$ lines on Si.

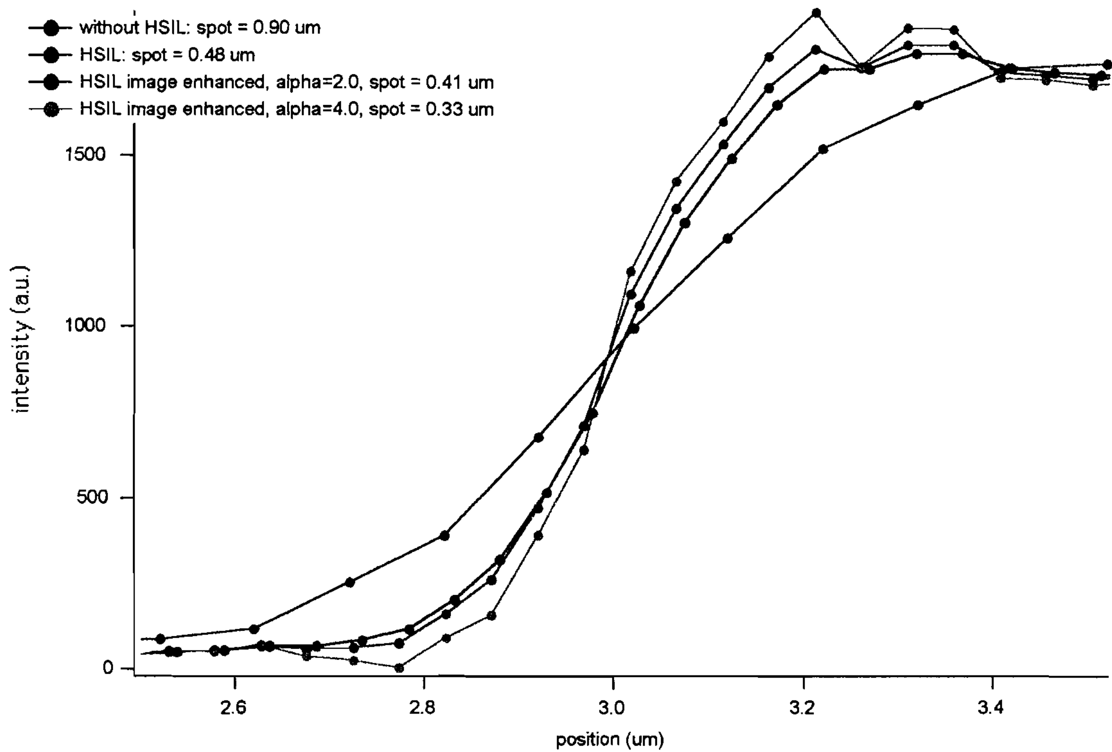

Fig. 2. Resolution enhanced scan over the $TiSi_2$ line border on Si.

§8.6 Two-dimensional formulation

When we look at a real two-dimensional image, instead of the scanned line we discussed before, all vectors become matrices. The image pixels can be represented by values in object and image matrices. The PSF also becomes two-dimensional, and the resulting convolution integral as well:

$$E(x,y) = \iint_{\xi,\eta} h(x-\xi, y-\eta) I(\xi,\eta) d\xi d\eta .$$

In this case the matrix **M** becomes very large, even for small values of n, so the calculation has to be restricted to pixels which are in the neighborhood of the pixel on which the operation is performed. The same calculations are used, they only become more elaborate. But also for complete images blurred by a PSF, image restoration has much to offer.

§8.7 micro-Raman spectroscopy stress measurements with high emphasis

Until now, we only considered the intensity of a signal. Of course, when we are looking at microscope images, this is certainly a useful thing to do, but real Raman data consist of localized peak position shifts. Fortunately, there is no reason why we should not be able to apply the same algorithm to Raman mechanical stress data. We can take the fitted curve peak position and apply the algorithm much in the same way as we did for the

intensity. Alternatively, we can take the complete spectrum, and apply the algorithm by adding complete spectra to each other after having multiplied them by the appropriate term from eq. (1). Afterwards, we can still do the curve-fitting, but now with the restored spectra. This is certainly advantageous, because correction on the fitted data will not, for example, take into account the peak broadening which takes place when the Raman peak shift is not the same for the entire area the spot is probing at one measuring point. So we have to consider the complete spectrum as a vector, and not only the intensity or Raman shift as one parameter. If we do so, of course the computation time will increase, but it is assumed that it will still remain acceptable.

PART THREE
Proposals for future investigation

CHAPTER NINE
Time discriminating TIVA with a short wavelength laser

§9.1 The principle of TIVA imaging

Temperature Induced Voltage Alteration basically uses the same measurement setup as in LIVA imaging, but the laser is replaced with a long wavelength one, so no carriers can be generated by photons with a higher energy than the bandgap, because they are not availible. However, when the laser beam is focused at the sample, heat will be generated, and so carriers are generated, because of the thermocouple effect. Two different conductors will, when connected together, give rise to a potential gradient. This effect is very weak, and when a metal line is connected to low resistance source such as a transistor or a power bus, the effect will be compensated for almost immediately.
When a conductor connected to a transistor gate is floating, e.g. due to a open circuit, the charge will remain and alter the working point of the transistor. This effect is amplified in the same way as for LIVA, the IC itself acting as the detector/amplifier. This effect is much smaller than the LIVA signals generated by a short wavelength laser, so care has to be taken that no light is emitted by the laser which has a wavelength for which the silicon α (defined in chapter 7) is large. The other process taking place when heating the sample with the laser beam, is resistance change in metal lines. When a short circuit is present, the current through the short depends on the resistance of this short. This resistance is altered by the temperature change, and a TIVA signal can be observed.
Although the inventors of TIVA, at Sandia [4], reserve the name TIVA for the latter measurement, and call the first SEI, Seebeck Effect Imaging, this is confusing. Both effects are observed at the same time and are indistinguishable when measuring. Only the fault determination step using electron microscopy or focused ion beam investigation will show which type of effect is observed. A very useful property of TIVA is that the metal lines causing the defect are visible, and not the transistors connected to it, like in LIVA.

§9.2 Recombination of excess carriers

The interesting question is now: Can we use a short wavelength laser for the TIVA measurements? This is the case if the light induced excess carriers recombine faster than the light generated thermal gradient vanishes. Then we can turn off the laser, first let the light-induced carriers disappear, and then sample the remaining TIVA signal.
We consider a piece of doped, for example p-type, silicon, on which light is incident. Apart from the thermally generated carriers $n_0(T)$ and $p_0(T)$ due to the device temperature, excess carriers are generated by the light. When the light is switched on, the concentration will increase, but after a while a new equilibrium will be reached. The concentration of electrons and holes is by then $n_0 + \delta n$ and $p_0 + \delta p$.
Now the light is switched off again and the carriers will effectively recombine until the thermal equilibrium condition is reached once more. We take the results of the derivation from [14, p. 195] under low level conditions, which means that the amount of generated excess carriers is small compared to the thermally generated majority carrier concentration p_0. This process is described by the differential equation

$$\frac{d\delta n(t)}{dt} = -\alpha_r p_0 \delta n(t).$$

In this equation α_r is the generation/ recombination rate of the intrinsic carriers. The solution to this equation is

$$\delta(t) = \delta n(0)e^{-\alpha_r p_0 t} = \delta n(0)e^{-t/\tau_{light}}$$

in which we call $\tau_{light} = 1/\alpha_r p_0$ the time constant of the excess carriers. This constant becomes very small for high doping concentrations. So if we know the material parameter α_r and the doping concentration p_0, we can calculate the intensity at every time after the light has been switched off.
Now we also have to consider the time-dependent distribution of the device temperature, which is higher than the room temperature due to the localized laser heating.
For the short wavelength approach to be useful, this temperature gradient should stay longer than it takes for the excess carriers to recombine. This means that the time constant of the temperature profile should be longer than that of the excess carriers. This is the case if doping concentrations are significant.

§9.3 Implementation of the TD-TIVA approach

With the theory from the previous paragraph, we are able to develop a Time Discriminating (TD-) variant of TIVA. We have to sample the TIVA voltage after the excess carriers generated by the incident light have vanished, but before our temperature gradient is gone also. We do not really know τ_{light} or $\tau_{thermal}$, because they both depend on the structure we are investigating. For that reason we need an adjustable delay time between the end of the illumination period and the sampling time, so we can look ourselves for the time delay which gives the best signal.
For the illumination we use the same laser as in the LIVA setup, but we add a “chopper” to obscure the heating beam half of the time. With a beam splitter, a part of the “chopped” light enters a photodetector, after which is determined whether the beam is obscured or not. This is the synchronization signal, which is amplified and delayed to trigger the sampling circuit at the right moment. A high speed pre-sample stage is used, because an ordinary high resolution A/D converter like the 16 bit one in the control electronics cannot complete a conversion within the short time the signal is available. It samples the signal, and holds this on its output until the A/D has performed a full cycle. We need a very sensitive preamplifier, because the signal levels are much lower than with LIVA.
The main disadvantage of TD-TIVA compared to ints conventional counterpart with an IR-laser, is that it cannot be used for “flip-chip” packaged devices, because the short wavelength laser light cannot penetrate the silicon substrate to reach the electronic structures.

CHAPTER TEN
Blind deconvolution

§10.1 Introduction
The main problem with the algorithm in the deconvolution chapter is the fact that accurate knowledge about the point spread function (PSF) is needed to obtain a reasonable improvement. In real laboratory circumstances the PSF is not known, because most interesting samples cannot be used for adequately measuring the spot size. Using a reference sample is no solution, because defocusing for putting our real object under the microscope instead of the reference is already enough to spoil our just determined spot. In this case it is possible to use a blind deconvolution algorithm, which determines the restored image *and* the PSF simultaneously from our data. Although computation times are long because this algorithm is iterative by nature, the results are hardly worse than the results of its non-blind counterpart [11]. This provides us with the possibility to do a measurement, and automatically deblur the image as a standard procedure. Very impressive results have been achieved with small objects on a black background. In the astronomy it is already used often. Fig. 10.1 and fig. 10.2. show photographs of the Hubble telescope taken with the 1.6 m telescope at Air Force Maui optical Station. The first is one photograph, the second is a blind deconvolved one using 50 photographs to correct for seeing, the turbulence of the atmosphere. But the first results in microscopy are also available , by [11]. PSF correction seems to work so good that even a completely in the digital domain working "auto-focus" has been proposed [10]

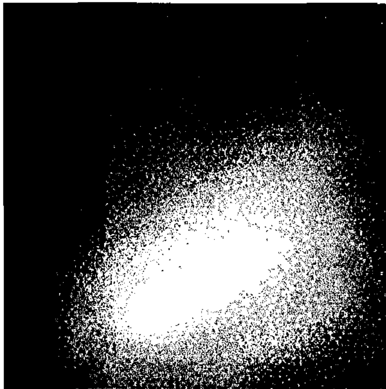

Fig 10.1 Hubble Telescope image

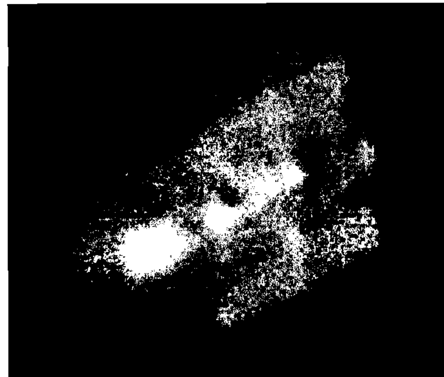

fig 10.2 Corrected by blind deconvolution

Figures taken from
http://www.ee.mtu.edu/faculty/schulz/research/blind_deconvolution.html

§10.2 Blind deconvolution for micro-Raman spectroscopy
For the algorithm to converge an image is needed with intensity differences. The algorithm cannot work with the stress data, so we have to feed it with the intensity data. What we can do, however, is using the intensity data for the blind deconvolution, but at the same time do the same calculations with the Raman stress data. In that way, the Raman stress data will be deblurred along with the intensity image. The best results are

obtained with small object on a dark background, as is the case in astronomy and fluorescent microscopy, but also for extended objects, the improvement should be substantial. Blind as well as non-blind algorithms will most likely be able to improve micro-Raman spectroscopy resolution well into the sub-0.5 micron region, especially if it is combined with near field effects like an oil immersion or solid immersion lens [22], [18].

CHAPTER ELEVEN
Kerr Rotation based Current Measurement (KRCM)

§11.1 Basic principle
When a polarized light beam is reflected at the surface of a magnetic material, the polarization is changed a little. By measuring the difference between the incident polarization and the reflected polarization, it is possible to calculate the magnetization. With the Raman spectrometer equipment, it is possible to do measurements of this kind on a micrometer scale. If we spin a very thin layer of non-conductive magnetizable material on the surface of an IC (e.g. a ferrite suspension in an organic solvent), the layer is magnetized on a microscopic scale by the currents flowing through the IC. If the ferrite used is a "fast" one, the magnetization will even follow the rapid changes of the current flow in signal lines. By focusing our polarized laser beam to a small spot and observing the polarization of the reflected light, we can investigate these magnetizations, and hence the currents flowing in our IC.

§11.2 Resolution
With the micro-Raman spectrometer, the minimum resolution is about 0.5 micron when using an oil immersion lens. Better resolution can be obtained by implementing a near-field optical system. It was shown [17] that polarization is preserved by the probing near field tip. The resolution in the current measurement depends on the minimum distinguishable polarization change.

§11.3 Proposals for practical implementation
Because ferrite is not soluble in organic solvents (e.g. acetone), very small ferrite particles have to be made. When we suspend them in an organic solvent, they can be put on top of the IC surface as a thin film without the need for a ferrite solution. With a photoresist spinner the suspension can be spinned on top of the surface. The difference between a solution and a suspension is that in a solution the molecules or ions of the solid are completely separated, while a suspension contains small particles still containing numerous molecules or ions. After drying the IC is connected to the power source and we can have a look at the behavior of the IC to different input stimuli. For DC measurements the acquisition electronics of chapter 5 can be used. A high speed A/D system is needed to investigate the IC at higher frequencies.

PART FOUR
General conclusions

In a short overview of failure analysis techniques it has been shown that optical failure analysis techniques have much to offer for the localization of defects on an IC.
Due to the components used, a micro-Raman spectroscopy system can be used for optical failure analysis with minor modifications. The possibilities to use this micro-Raman system in optical failure analysis have been investigated, and some of the optical techniques have been applied to the system.

By moving the objective of an optical microscope through the focal plane with a piezo positioner, an intensity distribution can be obtained which is used for:
* A highly accurate auto-focus system for the micro-Raman measurements
* Height determination on the sample by a Lorenz curve fitting procedure
The height measurement is too time consuming at present, but the suggested improvements should lead to shorter acquisition times.

The acquisition electronics, developed for the control of the piezo objective positioner and phododetector readings of the auto-focus system, can also be used for Light Induced Voltage Alteration (LIVA) failure analysis imaging. The modified micro-Raman spectroscope is capable of performing very high spatial resolution LIVA imaging. Scans over a large area take a lot of time, but this might be lowered by having less spatial resolution and a change in the way the XY-stage with the sample is moved under the microscope.

It is shown that is might be possible, with a laser chopper and high speed acquisition electronics, to use the short wavelength laser of the micro-Raman system for Temperature Induced Voltage Alteration (TIVA) measurements, instead of the IR-laser which is typically used at present. The advantage is a much higher spatial resolution and less cost.

Spatial resolution of micro-Raman spectroscopy can be improved in the XY-plane by applying digital image enhancement (deconvolution) techniques to the measured data. By using blind deconvolution techniques it might be possible to obtain resolution enhanced micro-Raman images on a routine basis.

By using the Kerr effect, it should be possible to measure current flowing through metal lines on an IC by spinning a thin film on its surface and measuring the Kerr rotation with a laser and a microscope.

Appendix A.
The acquisition electronics circuit board

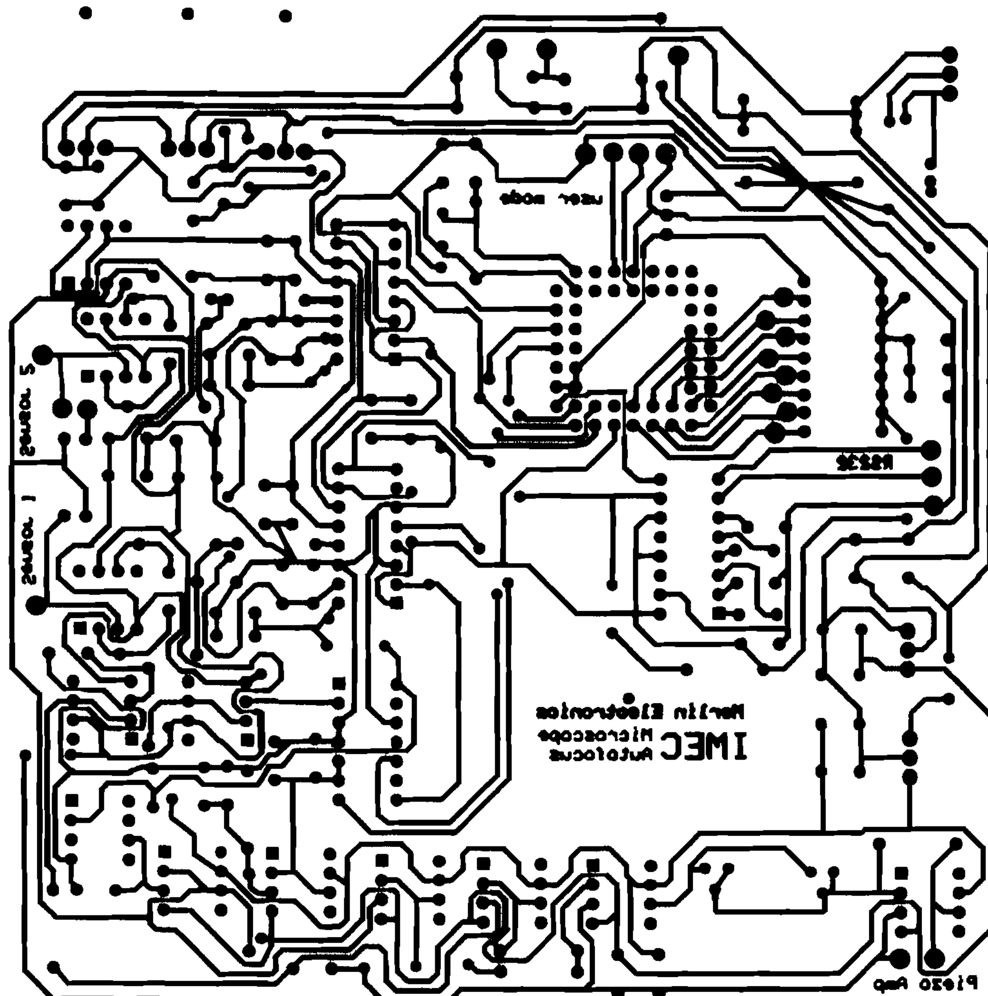

Appendix B.
Image reconstruction software

The image intensity restoration program

```
#include<stdio.h>
#include<assert.h>
#include<math.h>

void main(void)
{

        int i;
        float alpha, a,temp, temp2;
        char *filename="igor.txt";
        char *filename2="recon.txt";
        float g[15],tabel1[150],tabel2[150],tabel[150];
        FILE *file1;
        FILE *file2;


        printf("Merlin Electronics/IMEC\n");
        printf("PSF compenstation algorithm\n");
        printf("\nEnter spot size (Gaussian approximation) in micron: ");
        scanf("%f", &a);
        printf("\nEnter convolution correction factor: ");
        scanf("%f", &alpha);

        temp=-7.0;
        for(i=0;i<15;i++)      {
                temp2 = -(temp*temp/(15.0*a*a));
                g[i]=pow(2.7182818,temp2);
                temp=temp+1.0;
        }

        for(i=0;i<15;i++)
                printf("\n%f",g[i]);

        file1=fopen(filename,"r");
        assert(file1!=NULL);
        for(i=0;i<149;i++)
        fscanf(file1, "%f",&tabel2[i]);
        fclose(file1);

        for(i=0;i<149;i++)
                printf("%f\n",tabel2[i]);

        temp=0.0;
        for(i=0;i<15;i++)
        temp=temp+g[i];

        for(i=8;i<140;i++)
               tabel[i]=(1.0/temp)*(g[0]*tabel2[i-7]+g[1]*tabel2[i-6]+g[2]*tabel2[i-
               5]+g[3]*tabel2[i-4]+g[4]*tabel2[i-3]+g[5]*tabel2[i-2]+g[6]*tabel2[i-
               1]+g[7]*tabel2[i]+g[8]*tabel2[i+1]+g[9]*tabel2[i+2]+g[10]*tabel2[i+3]+g[11]
               *tabel2[i+4]+g[12]*tabel2[i+5]+g[13]*tabel2[i+6]+g[14]*tabel2[i+7]);

        for(i=17;i<130;i++)
                tabel1[i]=(alpha*tabel2[i]+(1-alpha)*tabel[i]);

        for(i=17;i<130;i++)
        printf("%f\n",tabel1[i]);

        file2=fopen(filename2,"w");
        assert(file2!=NULL);
        for(i=17;i<130;i++)
                fprintf(file2,"%f\n",tabel1[i]);
        fclose(file2);

        printf("\nFile recon.txt written correctly");
}
```

Appendix C.
Micro-Controller software

```
*********************************************************************
*                    Merlin Electronics/IMEC                        *
*            Microscope autofocus measurement software              *
*                          (c) 1998                                 *
*********************************************************************


*********************************************************************
*                          DEFINITIONS                              *
*********************************************************************


* Control Registers:

BASE                   EQU     $1000

PORTA                  EQU     $00      ; Port A data register
RESV1                  EQU     $01      ; Reserved
PIOC                   EQU     $02      ; Parallel I/O Control register
PORTC                  EQU     $03      ; Port C latched data register
PORTB                  EQU     $04      ; Port B data register
PORTCL                 EQU     $05      ;
DDRC                   EQU     $07      ; Data Direction register for port C
PORTD                  EQU     $08      ; Port D data register
DDRD                   EQU     $09      ; Data Direction register for port D
PORTE                  EQU     $0A      ; Port E data register
CFORC                  EQU     $0B      ; Timer Compare Force Register
OC1M                   EQU     $0C      ; Output Compare 1 Mask register
OC1D                   EQU     $0D      ; Output Compare 1 Data register

* Two-Byte Registers (High,Low -- Use Load & Store Double to access):

TCNT                   EQU     $0E      ; Timer Count Register
TIC1                   EQU     $10      ; Timer Input Capture register 1
TIC2                   EQU     $12      ; Timer Input Capture register 2
TIC3                   EQU     $14      ; Timer Input Capture register 3
TOC1                   EQU     $16      ; Timer Output Compare register 1
TOC2                   EQU     $18      ; Timer Output Compare register 2
TOC3                   EQU     $1A      ; Timer Output Compare register 3
TOC4                   EQU     $1C      ; Timer Output Compare register 4
TI4O5                  EQU     $1E      ; Timer In compare 4 or Out comp. 5
TCTL1                  EQU     $20      ; Timer Control register 1
TCTL2                  EQU     $21      ; Timer Control register 2
TMSK1                  EQU     $22      ; main Timer int Mask register 1
TFLG1                  EQU     $23      ; main Timer int Flag register 1
TMSK2                  EQU     $24      ; misc Timer int Mask register 2
TFLG2                  EQU     $25      ; misc Timer int Flag register 2
PACTL                  EQU     $26      ; Pulse Accumulator Control register
PACNT                  EQU     $27      ; Pulse Accumulator Count register
SPCR                   EQU     $28      ; SPI Control Register
SPSR                   EQU     $29      ; SPI Status Register
SPDR                   EQU     $2A      ; SPI Data Register
BAUD                   EQU     $2B      ; SCI Baud Rate Control Register
SCCR1                  EQU     $2C      ; SCI Control Register 1
SCCR2                  EQU     $2D      ; SCI Control Register 2
SCSR                   EQU     $2E      ; SCI Status Register
SCDR                   EQU     $2F      ; SCI Data Register
ADCTL                  EQU     $30      ; A/D Control/status Register
ADR1                   EQU     $31      ; A/D Result Register 1
ADR2                   EQU     $32      ; A/D Result Register 2
ADR3                   EQU     $33      ; A/D Result Register 3
ADR4                   EQU     $34      ; A/D Result Register 4
BPROT                  EQU     $35      ; Block Protect register
RESV2                  EQU     $36      ; Reserved
RESV3                  EQU     $37      ; Reserved
RESV4                  EQU     $38      ; Reserved
OPTION                 EQU     $39      ; system configuration Options
COPRST                 EQU     $3A      ; Arm/Reset COP timer circuitry
PPROG                  EQU     $3B      ; EEPROM Programming register
HPRIO                  EQU     $3C      ; Highest Priority Int and misc.
```

```
INIT                 EQU    $3D     ; RAM and I/O Mapping Register
TEST1                EQU    $3E     ; factory Test register
CONFIG               EQU    $3F     ; Configuration Control Register


* Interrupt Vector locations:

SCIINT               EQU    $D6    ; SCI serial system
SPIINT               EQU    $D8    ; SPI serial system
PAIINT               EQU    $DA    ; Pulse Accumulator Input Edge
PAOVINT              EQU    $DC    ; Pulse Accumulator Overflow
TOINT                EQU    $DE    ; Timer Overflow
TOC5INT              EQU    $E0    ; Timer Output Compare 5
TOC4INT              EQU    $E2    ; Timer Output Compare 4
TOC3INT              EQU    $E4    ; Timer Output Compare 3
TOC2INT              EQU    $E6    ; Timer Output Compare 2
TOC1INT              EQU    $E8    ; Timer Output Compare 1
TIC3INT              EQU    $EA    ; Timer Input Capture 3
TIC2INT              EQU    $EC    ; Timer Input Capture 2
TIC1INT              EQU    $EE    ; Timer Input Capture 1
RTIINT               EQU    $F0    ; Real Time Interrupt
IRQINT               EQU    $F2    ; IRQ External Interrupt
XIRQINT              EQU    $F4    ; XIRQ External Interrupt
SWIINT               EQU    $F6    ; Software Interrupt
BADOPINT             EQU    $F8    ; Illegal Opcode Trap Int
NOCOPINT             EQU    $FA    ; COP Failure (Reset)
CMEINT               EQU    $FC    ; COP Clock Monitor Fail
RESETINT             EQU    $FE    ; RESET Interrupt

* Data for serial port:

SPI_INIT             EQU    %01010000
DDRD_INIT            EQU    %00111010      ; D5 (SS) as a general output
BAUD1200             EQU    %00110011
BAUD9600             EQU    %00110000
TRENA                EQU    %00001100      ; Transmit, Receive ENAble
RDRF                 EQU    $20            ; Receive Data Register Full
TDRE                 EQU    $80            ; Transmit Data Register Empty

* data for AD and DA converters:

SENSOR1IN            EQU    %11111101      ; CS selects A/D 1
SENSOR2IN            EQU    %11110111      ; CS selects A/D 2
PIEZO_OUT            EQU    %11011111      ; CS selects D/A
CSOFF                EQU    $FF            ; CS selects none of them
position             RMB    2              ; 16 bit position code
number               RMB    2              ; adaptive focus counter
variableA            RMB    1              ; temporary 1 byte variable
counter              RMB    2
variableB            RMB    1
variableC            RMB    1
variableD            RMB    1
variableE            RMB    1
variableF            RMB    1
variableG            RMB    1
mode                 RMB    1              ; user mode number
intensity            RMB    2              ; 16 bit intensity code
position1            RMB    2
mean_position        RMB    2
threshold            RMB    2
offset               RMB    2
offset_temp          RMB    2
offsetA              RMB    2
*****************************************************************
*                    INITIALISATION                             *
*****************************************************************


        ORG          $F800                 ; first EEPROM adress
        LDS          #$00FF                ; set stack to top of internal RAM

* initialize serial port:

        LDX          #BASE                 ; X offset
        LDAA         #BAUD9600             ; communication at 9600 baud
        STAA         BAUD,X
        LDAA         #TRENA                ; TxD and RxD on
```

```
        STAA           SCCR2,X
        LDAA           SCSR,X

* configure port A pins used as outputs:

        LDAA           #$FF                  ; pin PA7 and PA3 as output
        STAA           PACTL,X

* configure port C pins as outputs:

        LDAA           #$FF
        STAA           DDRC,X

* configure port D as SPI and D5 (SS) as general output:

        LDAA           #SPI_INIT             ; turn on SPI
        STAA           SPCR,X
        LDAA           #DDRD_INIT            ; but leave D5 (SS) as output
        STAA           DDRD,X
        CLRA
        STAA           PORTD,X ; D5 = 0
        LDAA           SPSR,X

*       Initialize autofocus offset parameter
*
        LDD            #$0000
        STD            offset

* The MAX195 requires 14000 clock cycles to perform a calibration procedure. Both of
* the A/Ds are supplied with these clock pulses by writing the SPI 1750 times and
* throwing away the data.

* initialize A/D converters:

        LDAA           #SENSOR1IN
        STAA           PORTC,X
        LDY            #$036F                ; 14000/8=1750 times 8-bit word out
send1:  STAA           SPDR,X                ; read/write A/D and send 8 clk's to it
send2:  LDAA           SPSR,X
        BPL            send2
        DEY                                  ; 14000 clk's?
        BNE            send1
end_of_init1:
        LDAA           #SENSOR2IN
        STAA           PORTC,X
        LDY            #$036F                ; 14000/8=1750 times 8-bit word out
send3:  STAA           SPDR,X                ; read/write A/D and send 8 clk's to it
send4:  LDAA           SPSR,X
        BPL            send4
        DEY                                  ; 14000 clk's?
        BNE            send3

*********************************************************************
*                            MAIN PROGRAM                           *
*********************************************************************

        JMP            main
height:
        JSR            measure_height
        JMP            main
adaptive:
        JSR            adaptive_focus
        JMP            main
raman:  JSR            autofocus
        JMP            main
TIVA:   JSR            TIVAroutine
        JMP            main
light:  JSR            get_light


main:
        LDD            #$FFFF
        JSR            position_piezo
        JSR            receive_SCI
        STAA           mode
        JSR            send_SCI
        LDAA           mode
```

```
        CMPA            #'1'
        BEQ             height
        LDAA            mode
        CMPA            #'2'
        BEQ             adaptive
        LDAA            mode
        CMPA            #'3'
        BEQ             raman
        LDAA            mode
        CMPA            #'4'
        BEQ             TIVA
        LDAA            mode
        CMPA            #'5'
        BEQ             light
        BRA             main

*********************************************************************
*                       Subroutines                                 *
*********************************************************************

*********************************************************************
* Position_piezo sends the value stored in D to the piezo D/A.      *
*********************************************************************

position_piezo:
        PSHB
        PSHA
        LDAA            #PIEZO_OUT      ; CS of D/A forced low.
        STAA            PORTC,X
        PULA
        STAA            SPDR,X          ; Send MSB.
pos1:   LDAA            SPSR,X
        BPL             pos1            ; Transfer completed?
        PULB
        STAB            SPDR,X          ; Send LSB.
pos2:   LDAA            SPSR,X
        BPL             pos2            ; Transfer completed?
        LDAA            #CSOFF          ; CS high again.
        STAA            PORTC,X
        RTS

***********************************************************************************
* Readsensor1 forces CS of A/D 1 low and calls read. After the conversion is      *
* finished, CS is made high again.                                                *
***********************************************************************************

readsensor1:
        LDAA            #SENSOR1IN
        STAA            PORTC,X
        JSR             read
        PSHA
        LDAA            #CSOFF
        STAA            PORTC,X
        PULA
        RTS

***********************************************************************************
* Readsensor2 forces CS of A/D 2 low and calls read. After the conversion         *
*is finished, CS is made high again.                                              *
***********************************************************************************

readsensor2:
        LDAA            #SENSOR2IN
        STAA            PORTC,X
        JSR             read
        PSHA
        LDAA            #CSOFF
        STAA            PORTC,X
        PULA
        RTS

***********************************************************************************
* Read performs one conversion of the A/D and stores the resulting value in D. The *
* first 2 and the last 6 bits of the 3-byte transfer are not the conversion data,  *
* and are thrown away.                                                             *
***********************************************************************************
```

```
read:
        JSR             readAD
        PSHA
        JSR             readAD
        TAB
        PULA
        LSLD
        LSLD
        LSLD
        PSHA
        STAB            variableD
        JSR             readAD
        LSRA
        LSRA
        LSRA
        LSRA
        LSRA
        ORAA            variableD
        TAB
        PULA
        RTS


****************************************************************************
* ReadAD executes the instructions to get 8 bits of the SPI transfer in A. *
****************************************************************************

readAD:
        STAA            SPDR,X
read1:  LDAA            SPSR,X
        BPL             read1           ; wait until transfer finished
        LDAA            SPDR,X
        RTS

****************************************************************************
* Measure_height collects the intensity for all the 2^16 positions of the  *
* objective, and sends them to the host computer.                          *
****************************************************************************

measure_height:

mstart: JSR             receive_SCI
        CMPA            #'r'
        BNE             mstart
        JSR             send_SCI
        LDD             #$FFFF
        JSR             position_piezo
        JSR             readsensor1
        PSHB
        PSHA
        JSR             receive_SCI
        PULA
        JSR             send_SCI
        JSR             receive_SCI
        PULA
        JSR             send_SCI
        LDY             #$FFFF
mloop:  DEY
        STY             position
        XGDY
        JSR             position_piezo
        JSR             readsensor1
        PSHB
        PSHA
        JSR             receive_SCI
        PULA
        JSR             send_SCI
        JSR             receive_SCI
        PULA
        JSR             send_SCI
        LDY             position
        BNE             mloop
        RTS

*********************************************************************
```

```
adaptive_focus:
        JSR             receive_SCI
        CMPA            #'r'
        BNE             adaptive_focus
        LDD             #$FFFF
        STD             position
        JSR             position_piezo
        LDY             #$FFFF
aloop:  DEY
        BNE             aloop
        LDD             #$FFFF
adfloop:
        JSR             position_piezo
        LDY             position
        DEY
        STY             position
        JSR             readsensor1
        CMPA            #$FF                ; is the intensity below threshold?
        BEQ             adfloop

        LDD             position
        ADDB            #$02                ; go back 1024 positions
        STD             position
        PSHB
        JSR             send_SCI
        JSR             receive_SCI
        PULA
        JSR             send_SCI
        LDD             #12000
        STD             number
        LDY             number
adf:    DEY
        STY             number
        LDD             position
        JSR             position_piezo
        JSR             readsensor1
        PSHB
        PSHA
        JSR             receive_SCI
        PULA
        JSR             send_SCI
        JSR             receive_SCI
        PULA
        JSR             send_SCI
        LDY             position
        DEY
        STY             position
        LDY             number
        BNE             adf
        RTS

*******************************************************************

TIVAroutine:
        JSR             readsensor1
        PSHB
        PSHA
        JSR             receive_SCI
        PULA
        JSR             send_SCI
        JSR             receive_SCI
        PULA
        JSR             send_SCI
        RTS

***********************************************************************

get_light:
        JSR             readsensor2
        PSHB
        PSHA
        JSR             receive_SCI
        PULA
        JSR             send_SCI
        JSR             receive_SCI
        PULA
```

```
        JSR             send_SCI
        RTS

****************************************************************************
* Send_SCI sends the value stored in A (8 bit) to the host computer.       *
****************************************************************************
send_SCI:
        STAA            variableD
        JSR             UART_send
        JSR             UART_receive
        LDAA            variableD
        JSR             UART_send
        JSR             UART_receive
        LDAA            variableD
        JSR             UART_send
        RTS

UART_send:
        PSHA
sloop:  LDAA            SCSR,X              ; byte sent?
        BPL             sloop
        PULA
        STAA            SCDR,X              ; write first char to serial port
        RTS

****************************************************************************
* Receive_SCI waits until a byte is received and stores this byte in A     *
* Note that this is an 8 bit transfer.                                     *
****************************************************************************

recreturnG:
        LDAA            variableG
        RTS
get_another:
        JSR             UART_send
        JSR             UART_receive
        STAA            variableG
        CMPA            variableD
        BEQ             recreturnG
        LDAA            variableG
        CMPA            variableE
        BEQ             recreturnG
        LDAA            variableD
        RTS
receive_SCI:
        JSR             UART_receive
        STAA            variableD
        JSR             UART_send
        JSR             UART_receive
        STAA            variableE
        JSR             UART_send
        JSR             UART_receive
        STAA            variableF
        CMPA            variableE
        BNE             get_another
        LDAA            variableD
        CMPA            variableE
        BNE             get_another
        LDAA            variableE
        RTS

UART_receive:
        LDAA            SCSR,X
        ASLA
        ASLA
        BPL             UART_receive
        LDAA            SCDR,X
        RTS

************************************************************************************
* Determine_offset is used to correct for focusing to the wrong focal plane.       *
* First, the focus is found using autofocus. Then the user can change the focus    *
* with the focus knob. Afterwards the objective is again focused using autofocus.  *
* The difference between these two positions is stored in the variable "offset".  *
************************************************************************************

negative:
```

```
        ORAA            #%10000000
        STD             offset
        RTS

determine_offset:
        JSR             autofocus
        LDD             mean_position
        STD             offset_temp
        JSR             receive_SCI
        JSR             autofocus
        LDD             mean_position
        SUBD            offset_temp
        BMI             negative
        STD             offset
        RTS

*********************************************************************************
* The autofocus routine scans from two sides to the intensity peak which occurs    *
* near focus. The middle between the two "threshold"-intensities is taken as the   *
* objective position. This measurement is performed 32 times to correct for noise. *
* Because the amp corrects voor hysteresis there is no need to scan from one       *
* direction only.                                                                   *
*********************************************************************************

autofocus:
        JSR     receive_SCI
        CMPA    #'r'
        BNE     autofocus
        LDD     #$FFFF          ; initialization
        STD     position
        STD     mean_position
        JSR     position_piezo
        LDY     #$2FFF
auwacht:
        DEY
        BNE     auwacht
        LDD     #$FB00          ; first threshold value
        STD     threshold
        LDY     #$0001          ; 32 times
auloop:
        LDD     position
        SUBD    #$0002          ; change objective position
        STD     position
        JSR     position_piezo
        JSR     readsensor1
        CPD     threshold
        BGT     auloop
        LDD     position
        SUBD     #$00AF
        STD     mean_position

        LDD     #$0000
        STD     position1

        LDD     mean_position
        JSR     position_piezo  ; position objective in the right focal plane.
        JSR     send_SCI
        RTS

***************************************************************************

substract:
        LDD             offset
        ANDA            #%01111111
        STD             offsetA
        LDD             mean_position
        SUBD            offsetA
        RTS

add_offset:
        LDD             offset
        BMI             substract
        LDD             mean_position
        ADDD            offset
        RTS
```

```
*************************************************************************
       END
```

Appendix D.
Micro-Raman spectroscopy auto-focus software

The original Dilor micro-Raman spectroscopy software uses one big executable file as main program: OMA4P3.EXE. One of the C-files is PIFOC.C, which contains the function set_pifoc( ). This function is called for by the Raman soft, every time an auto-focus action has to be taken. It does the auto-focus work and gives back the control to another part of the program. When using a different auto-focus system, one only has to change the contents of this function to drive the new auto-focus system. Here we see the auto-focus function as used with the new system: it only initializes the COM2 port and sends a mode '3' command to the auto-focus module. The module does the auto-focusing all by itself. When the set_pifoc( ) function gets back the "ready" command from the auto-focus module, it returns to the calling function. Some other functions are given which are special versions with arguments of the Dilor set_pifoc( ). They are not used by the new system.

```
#include <dos.h>
#include <stdlib.h>
#include <string.h>
#include <time.h>
#include <conio.h>
#include <stdio.h>
#include <assert.h>

#define  UART_BASEADDR  0x2F8// the base address of the UART COM2 port.
                            // the UART COM1 adress is 0x3F8
#define  UART_BAUDRATE  12   // the BAUD register divisor value.
#define  UART_LCRVAL    0x1b // the value to be written to the LCR.
#define  UART_FCRVAL    0x87 // the value to be written to the FCR.


char UARTget()
{
        unsigned x = 0;
        while ((inp(UART_BASEADDR+5)&0x01)==0);

        x = (inp(UART_BASEADDR+5) & 0x9f) << 8;
        if (x&0x100) x|=((unsigned)inp(UART_BASEADDR))&0xff;
        return x;
}

void UARTput(char character)
{
        while ((inp(UART_BASEADDR+5)&0x20)==0);
        outp(UART_BASEADDR,(int)character);
}


unsigned UART_get_char()
{
        char byte0, byte1, byte2, byte3;

        byte0 = UARTget();
        UARTput('a');
        byte1 = UARTget();
        UARTput('a');
        byte2 = UARTget();
        if((byte0 == byte1) && (byte1 == byte2))
                return byte0;

        UARTput('a');
        byte3 = UARTget();
        if((byte1 == byte2) && (byte2 == byte3))
                return byte3;
```

```
        if((byte0 == byte1) && (byte1 == byte3))
                return byte0;
        if((byte0 == byte2) && (byte2 == byte3))
                return byte0;
        else return 0;
}

void UART_send(char byte)
{
        char dummy;

        UARTput(byte);
        dummy = UARTget();
        UARTput(byte);
        dummy = UARTget();
        UARTput(byte);
}


void set_pifoc(int func,float value)
{
        /* Main autofocus function */

        /* Initialization of serial port */
        outp(UART_BASEADDR+3,0x80);
        outpw(UART_BASEADDR,UART_BAUDRATE);
        outp(UART_BASEADDR+3,UART_LCRVAL);
        outp(UART_BASEADDR+4,0);

        /* Remove any word already in the data register */
        inp(UART_BASEADDR+5);
        inp(UART_BASEADDR);

        /* Send the start command to autofocus module */
        UART_send('3');

        /* Wait until autofocus algorithm is completed. */

        UART_get_char();
}

void pifoc_init()
{
 set_pifoc(1,50);
}

void set_autofocus()
{
 set_pifoc(0,0);
}
```

Appendix E.
Data acquisition software

This software does the height and LIVA/TIVA measurements. Very useful for this part was the information concerning file operations in [15].

```
#include <bios.h>
#include <dos.h>
#include <stdlib.h>
#include <string.h>
#include <time.h>
#include <stdio.h>
#include <conio.h>
#include <assert.h>

#define  UART_BASEADDR  0x2F8// the base address of the UART COM2 port.
#define  UART_BAUDRATE  12    // the BAUD register divisor value.
#define  UART_LCRVAL    0x1b // the value to be written to the LCR.

#define  UART_BASEADDR1 0x3F8 // the base address of the UART COM1 port.
#define  UART_BAUDRATE1 48
#define  UART_LCRVAL1  0x07
#define  UART_FCRVAL   0x7

char xback[10],mclstatus[6],xrel[9]="0000000",yrel[9]="0000000";
// The string send functions use COM1, the charcter send functions use COM2.

void UART_initCOM1()
{
       outp(UART_BASEADDR1+3,0x80);
       outpw(UART_BASEADDR1,UART_BAUDRATE1);
       outp(UART_BASEADDR1+3,UART_LCRVAL1);
       outp(UART_BASEADDR1+4,0);
       outp(UART_BASEADDR1+2, UART_FCRVAL);
}

void UART_init()
{
       outp(UART_BASEADDR+3,0x80);
       outpw(UART_BASEADDR,UART_BAUDRATE);
       outp(UART_BASEADDR+3,UART_LCRVAL);
       outp(UART_BASEADDR+4,0);
       outp(UART_BASEADDR+2, UART_FCRVAL);
}

void UART_send_string1(char *string)
{
       int i=0;
       do
       {
              while ((inp(UART_BASEADDR1+5)&0x20) == 0);
              outp(UART_BASEADDR1, (char)string[i++]);
       }
       while(string[i-1] !='\r' || !i);
}

void UART_send_string(char *string)
{
       int i=0,j=0;
       char dummy[20];
       do
       {
              while ((inp(UART_BASEADDR1+5)&0x20)==0);
              if(string[i]=='\007'){
              outp(UART_BASEADDR1, '\007');
              i++;}
              else
              outp(UART_BASEADDR1,(char)string[i++]);
              if(i==2 && string[i-1] != '\017' && string[i-1] !='\120' && string[i-1] !=
              '\015' && string[i-1] !='\016')printf("%c", string[i-1]);
       }
```

```
        while(string[i-1] != '\r' || !i);
}

void UART_get_string()
{
        unsigned char i='a';
        unsigned x=0;
        do
        {
                while ((inp(UART_BASEADDR1+5)&0x01)==0); //data ready?
                x = (inp(UART_BASEADDR1+5) & 0x9f) << 8; //FIFO error?
                if (x&0x100) i=x|=((unsigned)inp(UART_BASEADDR1))&0xff;
        }
        while (i!='\r');
}


char UARTget()
{
        unsigned x = 0;
        while ((inp(UART_BASEADDR+5)&0x01)==0);
        x = (inp(UART_BASEADDR+5) & 0x9f) << 8;
        if (x&0x100) x|=((unsigned)inp(UART_BASEADDR))&0xff;
        return x;
}

void UARTput(char character)
{
        while ((inp(UART_BASEADDR+5)&0x20)==0);
        outp(UART_BASEADDR,(int)character);
}


unsigned UART_get_char()
{
        char byte0, byte1, byte2, byte3;

        byte0 = UARTget();
        UARTput('a');
        byte1 = UARTget();
        UARTput('a');
        byte2 = UARTget();
        if((byte0 == byte1) && (byte1 == byte2))
                return byte0;

        UARTput('a');
        byte3 = UARTget();
        if((byte1 == byte2) && (byte2 == byte3))
                return byte3;
        if((byte0 == byte1) && (byte1 == byte3))
                return byte0;
        if((byte0 == byte2) && (byte2 == byte3))
                return byte0;
        else return 0;
}

void UART_send(char byte)
{
        char dummy;

        UARTput(byte);
        dummy = UARTget();
        UARTput(byte);
        dummy = UARTget();
        UARTput(byte);
}

void enable_joystick()
{
 UART_send_string("U\007j\r");
 UART_send_string("U\120");
}

void disable_joystick(void)
{
        UART_send_string("j\r");
        UART_get_string();
```

```
}

void init_xy(void)
{
        UART_send_string("U\007c\r");
        UART_send_string("U\120\r");
        UART_get_string();
}


void move_plate(char *xpos,char *ypos)
{
        char str1[20],str2[20];

        strcpy(str1,"U ");
        strcpy(str2,"U\001");
        strcat(str1,xpos);
        strcat(str1,"\r");
        str1[1]=0;
        strcat(str2,ypos);
        strcat(str2,"\r");

        UART_send_string1("U\007v\r");
        UART_send_string1(str1);
        UART_send_string1(str2);
        UART_send_string1("U\120\r");
        UART_get_string();
}

void make_intensity_file(char *filename)
{
        char intensity;
        FILE *fid;
        unsigned int counter,x;
        unsigned int counter2, counter3=0;

        fid = fopen(filename, "wb");
                assert(fid != NULL);
        /* Remove any word already in the data register */
        inp(UART_BASEADDR+5);
        inp(UART_BASEADDR);

        UART_send('1');
        UART_get_char();
        UART_send('r');
        UART_get_char();

        for(counter2=0;counter2<512 ;counter2++)
        {
                printf("\r     %d", counter2);
                for(counter=0;counter<256;counter = counter+2)
                {
                        UART_send('a');
                        intensity = UART_get_char();
                        counter3++;
                        fprintf(fid, "%c", intensity);
                        UART_send('b');
                        intensity = UART_get_char();
                        counter3++;
                        fprintf(fid, "%c", intensity);
                }
        }

        fclose(fid);

}

void measure_voltage(char *filename)
{
        FILE *fid;
        char voltage;
        /* Remove any word already in the data register */
        inp(UART_BASEADDR+5);
        inp(UART_BASEADDR);

        /* Send the LIVA/TIVA start command to autofocus module */
        UART_send('4');
```

```
        UART_get_char();
        fid = fopen(filename, "a");
        UART_send('a');
        voltage = UART_get_char();
        fprintf(fid, "%c", voltage);
        UART_send('b');
        voltage = UART_get_char();
        fprintf(fid, "%c", voltage);
        fclose(fid);
}

void measure_voltage_and_light(char *filename)
{
        FILE *fid;
        char voltage, light;

        // Get voltage

        inp(UART_BASEADDR+5);
        inp(UART_BASEADDR);
        UART_send('4');
        UART_get_char();
        fid = fopen(filename, "a");
        UART_send('a');
        voltage = UART_get_char();
        fprintf(fid, "%c", voltage);
        UART_send('b');
        voltage = UART_get_char();
        fprintf(fid, "%c", voltage);

        // Get reflected light intensity

        UART_send('5');
        UART_get_char();
        UART_send('a');
        light = UART_get_char();
        fprintf(fid, "%c", light);
        UART_send('b');
        light = UART_get_char();
        fprintf(fid, "%c",light);
        fclose(fid);
}


void adaptive_focus_file(char *filename)
{
        char intensity, first_position, second_position;
        FILE *fid;
        unsigned int counter;

        fid = fopen(filename, "wb");
                assert(fid != NULL);

        UART_send('2');
        UART_get_char();
        UART_send('r');

        /* The first two bytes received are the starting point of */
        /* the intensity measurement. Then 12000 points are collected */

        first_position = UART_get_char();
        UART_send('r');
        second_position = UART_get_char();
        fprintf(fid,"%c", first_position);
        fprintf(fid,"%c", second_position);

        for(counter=0;counter<12000;counter = counter+1)
                {
                        UART_send('a');
                        intensity = UART_get_char();
                        printf("\r  %4d  %5u",intensity, counter);
                        fprintf(fid, "%c", intensity);
                        UART_send('b');
                        intensity = UART_get_char();
                        fprintf(fid, "%c", intensity);
                }
```

```
        fclose(fid);
}

void main (void)
{
        /* Main autofocus or measurement function */

        char filename[12]={'i','n','t','y','0','0','0','.','m','e','0'};
        int counter, files_total, mode_type, x;
        unsigned int i,j;
        long int xstep, ystep, xdistance, ydistance;
        char filenameLIVA[12], *string, chardummy;
        long int a,dummy, hours, minutes;

        printf("\n\n    Universal micro-Raman spectroscope data acquisition software\n");
        printf("                    Merlin Electronics/IMEC version 1.4\n\n");
        printf("    Position scanning possibilities:\n");
        printf("       (1) Complete area height scan\n");
        printf("       (2) Adaptive focus area height scan\n");
        printf("        (3) Micro-Raman autofocus\n");
        printf("        (4) LIVA/TIVA imaging\n");
        printf("       (5) LIVA/TIVA imaging with reflected light scan\n\n");
        printf("    Scan type: ");
        scanf("%d", &mode_type);

        if(mode_type != 1 && mode_type != 2 && mode_type != 3 && mode_type != 4 &&
mode_type != 5){
                        printf("    No such scanning mode, program aborted.\n");
                        exit(0);
                }
/* This part does not apply for the LIVA/TIVA mode */
if(mode_type != 4 && mode_type !=5)
{
        UART_init();
        UART_initCOM1();

        /* Resolution 0.1 micron */
        UART_send_string("U\0171\r");
        UART_send_string("U\01510000\r");
        UART_send_string("U\01610000\r");
        enable_joystick();
        disable_joystick();
        printf("    Calibrating XY-stage...");
        init_xy();

        printf("\r                                        \r");
        enable_joystick();
        init_xy();

        printf("    Number of accumulations: ");
        scanf("%d", &files_total);
        if(files_total > 999){
                printf("    Maximum number of accumulations is 999, program aborted\n");
                exit(0);
        }
        printf("    Scan length x direction (µm):         ");
        scanf("%ld", &xdistance);
        printf("    Step size in the x direction (.1 µm): ");
        scanf("%ld", &xstep);
        printf("    Scan length y direction (µm):         ");
        scanf("%ld", &ydistance);
        printf("    Step size in the y direction (.1 µm): ");
        scanf("%ld", &ystep);
        scanf("%c", &dummy);

        if( mode_type == 1)
                a = (files_total*xdistance*ydistance*100*360)/(xstep*ystep);
        if( mode_type == 2)
                a = (files_total*xdistance*ydistance*100*60)/(xstep*ystep);
        hours = a/(3600);
        minutes = ((a-hours*3600)/60);

        printf("    This scan will take approx. %d h %d m. Continue (y/n):", hours,
minutes);
        scanf("%c", &chardummy);
        if(chardummy != 'y'&& chardummy !='Y')
```

```
        {
                printf("\n    Program aborted by user.");
                exit(0);
        }

        printf("    Position the spot at the right-bottom corner of the scan area\n ");
        printf("   and press any key when ready.");
        scanf("%c", &dummy);
        scanf("%c", &dummy);
        printf("\r                             Number of y-axis scans:    0\r");
        disable_joystick();
        xdistance = xdistance*10;
        ydistance = ydistance*10;
        for(i=0;i<ydistance;i=i+ystep)
        {
                for(j=0;j<xdistance;j=j+xstep)
                {
                        sprintf(xrel,"%#0.7d", xstep);
                        move_plate(xrel,"0000000");

                    for(counter = 0; counter< files_total; counter++){

                        if(filename[4]=='9' && filename[5]=='9' && filename[6]=='9'){
                                printf("\n Too many files");
                                exit(0);
                        }
                        else if(filename[5]=='9' && filename[6]=='9'){
                                filename[6]='0';
                                filename[5]='0';
                                filename[4]++;
                        }
                        else if(filename[6]=='9'){
                                filename[6]='0';
                                filename[5]++;
                        }
                        else    filename[6]++;
                        if(mode_type == 1)
                                filename[10] = '1';
                        if(mode_type == 2)
                                filename[10] = '2';


                                if(mode_type == 1)
                                        make_intensity_file(filename);
                                if(mode_type == 2)
                                        adaptive_focus_file(filename);
                        }
                }
                sprintf(xback,"-%#0.7d",xdistance);
                sprintf(yrel,"%#0.7d",ystep);
                move_plate(xback,yrel);
                printf("                              Number of y-axis scans: %3d\r",
(i/ystep)+1);
        }
        printf("\n\n    Measurement completed succesfully.");
}
/* This part is only for the LIVA/TIVA mode */
if(mode_type == 4 || mode_type == 5)
{

        printf("    Enter name of the LIVA/TIVA output file: ");
        scanf("%s", &filenameLIVA);
        UART_init();
        UART_initCOM1();

        /* Resolution 0.1 micron */
        UART_send_string("U\0171\r");
        UART_send_string("U\01510000\r");
        UART_send_string("U\01610000\r");
        enable_joystick();
        disable_joystick();
        printf("    Calibrating XY-stage...");
        init_xy();

        printf("\r                                     \r");
        enable_joystick();
        init_xy();
```

```
        printf("    Scan length x direction (µm):          ");
        scanf("%ld", &xdistance);
        printf("    Step size in the x direction (.1 µm): ");
        scanf("%ld", &xstep);
        printf("    Scan length y direction (µm):          ");
        scanf("%ld", &ydistance);
        printf("    Step size in the y direction (.1 µm): ");
        scanf("%ld", &ystep);
        scanf("%c", &dummy);

        a = (xdistance*ydistance*100)/(xstep*ystep*5);
        hours = a/(3600);
        minutes = ((a-hours*3600)/60);

        printf("    This scan will take approx. %ld h %ld m. Continue (y/n):", hours,
minutes);
        scanf("%c", &chardummy);
        if(chardummy != 'y'&& chardummy !='Y')
        {
                printf("\n    Program aborted by user.");
                exit(0);
        }

        printf("    Position the spot at the right-bottom corner of the scan area\n ");
        printf("   and press any key when ready.");
        scanf("%c", &dummy);
        scanf("%c", &dummy);

        printf("\n\r    Number of y-axis scans:   0 \r");
        disable_joystick();
        xdistance = xdistance*10;
        ydistance = ydistance*10;
        for(i=0;i<ydistance;i=i+ystep)
        {
                for(j=0;j<xdistance;j=j+xstep)
                {
                        sprintf(xrel,"%#0.7ld", xstep);
                        move_plate(xrel,"0000000");
                        if(mode_type == 4)
                                measure_voltage(filenameLIVA);
                        if(mode_type == 5)
                                measure_voltage_and_light(filenameLIVA);
                }
                sprintf(xback,"-%#0.7ld",xdistance);
                sprintf(yrel,"%#0.7ld",ystep);
                move_plate(xback,yrel);
                printf("    Number of y-axis scans: %3d\r", (i/ystep)+1);
        }
        printf("\n    Measurement completed succesfully.\n");
}


}
```

Acknowledgements

This study was carried out as a graduate thesis at IMEC (Inter-university Micro-Electronic Center), Leuven (Belgium). I would like to thank my supervisor Ingrid De Wolf for her everlasting enthusiasm (even at times I couldn't see why) and help. Thanks a lot! Furthermore, I would like to thank Paul Tielemans for the help he gave me by e-mail about the C-programming part. Bram van Straaten, Allert van Zelst, Erik Brockmeyer, Michiel Esvelt and Marc van Heijningen helped me feeling quite at ease in Leuven. Finally, I would like to thank Lode Vandamme, my coordinator in Holland from Eindhoven University of Technology, and prof. Rudy van der Plasse for the fact that they gave me the chance to finish my study at IMEC in Leuven.

References

[1] Barton, D. L. and P. Tangyunyong, ***Fluorescent microthermal imaging - Theory and methodology for achieving high thermal resolution images***, Microelectronic enigineering 31 (1996) 271-279.
[2] Cohen, D.K., W. H. Gee, M. Ludeke and J. Lewkowicz, ***Automatic focus control: the astigmatic lens approach***, Applied optics, Vol 23 (1984), No. 4, 565-570.
[3] Cole, E. I. Jr., ***Electron and optical beam testing of integrated circuits using CIVA, LIVA and LECIVA***, Microelectronic engineering 31 (1996) 13-24.
[4] Cole, E. I. Jr, P. Tangyunyong and D. L. Barton, ***Backside Localization of open and shorted IC interconnections***, IEEE 98CH36173. 36th annual international reliability physics symposium, Reno, Nevada, 1998, 129-136.
[5] Frankowski, G., ***Optisches 3D-Meßsystem zur Mikroprofil und Rauheitsmessung***, F&M, 106 (1998), No. 9, 612-615.
[6] Grasserbauer, M. and H. W. Werner (editors), ***Analysis of microelectronic materials and devices***, John Wiley and sons, Chichester, 1991
[7] ***HC11***, *M68HC11 E series, HCMOS microcontroller unit,* Technical data, MC68HC11E/D rev 1, Motorola Inc., 1995.
[8] van der Heijden, F. ***Image based measurement systems***, *object recognition and parameter estimation*, John Wiley & Sons Ltd., Chichester, 1994.
[9] Hellen, E. H. and D. Axelrod. ***An automatic focus/hold system for optical microscopes***, Rev. Sci. Instrum. 61 (12), December 1990, 3722-3725.
[10] Kim, S. K. and J. K. Paik, ***Out-of-focus blur estimation and restoration for digital auto-focusing system***, Electronics letters, Vol 34 (1998), No. 12, 1217-1219.
[11] Krishnamurthi, V., Y. Liu, S. Bhattacharyya, J. N. Turner and T. J. Holmes, ***Blind deconvolution of fluorescence micrographs by maximum-likelihood estimation***, Applied optics, Vol 34 (1995), No. 29, 6633-6647.
[12] Mason, D. C. and D. K. Green, ***Automatic focusing of a computer-controlled microscope***, IEEE transactions on biomedical engineering, vol MBE-22, No. 4, July 1975.
[13] Nakajima, S. , T. Ueki, Y. Shionoya, K. Mafune, N. Kuji, S. Nakamura, Y. Komine and T. Takeda, ***Current status of failure analysis for ULSI's***, Proc. 21st international conference on microelectronics (MIEL'97), Vol. 2, Nis, Yugoslavia, 1997, 591-598.
[14] Neamen, D. A., ***Semiconductor physics and devices***, *Basic principles*, IRVIN, Burr Ridge, 1992.
[15]Nikawa, K., C. Matsumoto and S. Inoue, ***Novel method for defect detection in Al stripes by means of laser beam heating and detection of changes in electrical resistance***, Jpn. J. Appl. Phys., Vol 34 (1995), 2260-2265.
[16] Paredaens, J. , P. de Bra and H. Olivie, ***Leren programmeren met C***, Kluwer Bedrijfswetenschappen, Deventer, 1992, ISBN 90 267 17083.
[17] Pohl, D. W. And D. Cordjon (editors), ***Near field optics***, NATO ASI Series, Series E: Applied Sciences – Vol. 242, Kluwer academic Publishers, Deventer, 1993.
[18] Poweleit, C. D., A Gunther, S. Goodnick and J. Menendez, ***Raman imaging of patterned silicon using a solid immersion lens***, Appl. Phys. Lett., Vol 73 (1998), No. 16, 2275-2277.

[19] Press, W. H., B. P. Flannery, S. A. Teukolsky and W. T. Vetterling
Numerical recipes in C, Cambridge University Press, Cambridge, 1990.
[20] Self, S. A. ,***Focusing of spherical Gaussian beams***, Applied optics, Vol 22, No. 5 (1983), 658-661.
[21] Soden, J. M. and R. E. Anderson, ***IC failure analysis: techniques and tools for quality and reliability improvement***, Microelectron. Reliab. Vol 35 (1995), No. 3, 429-453.
[22] van Spengen, W. M., ***Submicron spatial resolution in micro-Raman spectroscopy with the solid immersion lens.*** , IMEC internal report, IMEC, Kapeldreef 75, Leuven (Belgium), 1998.
[23] De Wolf, I., H. E. Maes and S. K. Jones, ***Stress measurements in silicon devices through Raman spectroscopy: Bridging the gap between theory and experiment***, J. Appl. Phys. 79(9), 1996, 7148-7156.
[24] De Wolf, I. ,***Micro-Raman spectroscopy to study local mechanical stress in silicon integrated circuits***, Semicond. Sci. Technol. 11 (1996), 139-145.